

## Effects of a resonant cavity on macroscopic quantum tunneling of fluxons in long Josephson junctions

Ju H. Kim and Ramesh P. Dhungana\*

*Department of Physics and Astrophysics, University of North Dakota, Grand Forks, North Dakota 58202-7129, USA*

(Received 29 July 2010; revised manuscript received 6 October 2010; published 9 February 2011)

We investigate the effects of a high-quality resonant cavity on macroscopic quantum tunneling (MQT) of fluxons from both a metastable state to continuum and from one degenerate ground state of a double-well potential to the other. By using a set of two coupled perturbed sine-Gordon equations, we describe the tunneling processes in linear long Josephson junctions and find that MQT in the resonant cavity increases due to potential renormalization, induced by the interaction between the fluxon and the cavity. Enhancement of the MQT rate in the weak-coupling regime is estimated by using the experimentally accessible range of the model parameters. The tunneling rate from the metastable state is found to increase weakly with increasing junction-cavity interaction strength. However, the energy splitting between the two degenerate ground states of the double-well potential increases significantly with increasing both the interaction strength and the frequency of the resonant cavity mode. Finally, we discuss how the resonant cavity may be used to tune the property of Josephson vortex quantum bits.

DOI: [10.1103/PhysRevB.83.064503](https://doi.org/10.1103/PhysRevB.83.064503)

PACS number(s): 74.50.+r, 74.78.Na, 85.25.Cp

### I. INTRODUCTION

Experimentally observed<sup>1</sup> quantum behavior of Josephson vortices (i.e., fluxons) at ultralow temperatures has opened up a possibility of realizing quantum computers based on long Josephson junctions (LJJ's). This observation led to much interest in the Josephson vortex quantum bit<sup>2-4</sup> (qubit) as an alternative to the previously proposed superconducting qubits. Similar to other approaches based on Josephson junctions, such as charge,<sup>5</sup> phase,<sup>6</sup> and flux<sup>7</sup> qubits, the Josephson vortex qubit (JVQ) is also a promising candidate for quantum computation application. Due to its weak interaction with decoherence sources in the environment at low temperatures, the JVQ may have significant advantages over the other superconducting qubits. For instance, a significantly longer decoherence time was suggested as one such advantage.<sup>3</sup>

The JVQ takes advantage of the coherent superposition of two spatially separated states arising from the low-temperature property of a trapped fluxon in a double-well potential. This property includes (i) energy quantization and (ii) macroscopic quantum tunneling<sup>1</sup> (MQT). We note that, for linear LJJ's, the fluxon potential for either the metastable state or the JVQ may be obtained<sup>8</sup> by using Nb-AlO<sub>x</sub>-Nb junctions and by implanting either one or two microresistors in the insulator layer, respectively. For application of JVQ's, tuning both the decoherence time and the level of entanglement by controlling the qubit property is essential. However, due to its weak interaction with external perturbations, an effective tuning mechanism for the JVQ is less clear. Recent studies<sup>9,10</sup> on using a microwave cavity for both tuning a single-phase qubit and inducing an interaction between either two charge or two phase qubits suggest that a resonant cavity may be used for the JVQ to serve the same purpose.

Earlier studies on the effects of a resonant cavity indicate<sup>11,12</sup> that both electric and magnetic fields of the cavity couple to the Josephson junction since the cavity electromagnetic (EM) mode behaves similarly to a phonon mode,<sup>13</sup> which interacts with the fluxon. The effects of a resonant cavity on the fluxon dynamics in LJJ stacks<sup>14-16</sup> have been studied both experimentally<sup>17,18</sup> and theoretically.<sup>19-21</sup>

These studies show that when the coupling between the LJJ and a resonant cavity is spatially uniform, no force is exerted on the fluxon by the cavity, but its dynamics may become modified. These studies suggest that the interaction between the LJJ and a resonant EM wave mode of the cavity promotes<sup>22</sup> collective dynamics of fluxons. The in-phase locking mode of the fluxon dynamics is shown to be enhanced<sup>22</sup> by the cavity EM mode.

These studies also suggest that the junction-cavity interaction may be used to change the qubit property. The property of the JVQ depends on MQT between two spatially separated states of the fluxon. We note that MQT represents quantum-particle-like collective excitations.<sup>23,24</sup> As semiclassical theories indicate that the MQT rate<sup>25</sup> depends on the potential barrier height, the JVQ can be tuned by adjusting the potential well for the fluxon. This adjustment can be achieved by potential renormalization induced by the junction-cavity interaction since this interaction can strongly affect the fluxon tunneling processes, similar to phonon-assisted tunneling in Josephson junctions.<sup>26</sup> We note that a two-level atom interacting with a quantized radiation field, described by the Jaynes-Cummings model,<sup>27</sup> is also similar to the JVQ-cavity system that we consider in the present work. The potential renormalization for fluxons suggests that the resonant cavity may be used as a tool for controlling the JVQ property. As the fluxon tunneling processes may be controlled externally by tuning either the junction-cavity coupling strength or the resonant frequency, the effects of the resonant cavity depend on the nature of the interaction. However, the influence of the junction-cavity interaction on the MQT rate has not been understood clearly.

In this paper, we investigate the effects of the junction cavity both on MQT from a metastable state and on the ground-state energy splitting in a double-well potential. We note that, to focus on the interaction between the LJJ and a single resonant cavity mode, we consider only a high-quality ( $Q_c$ ) cavity. First, we estimate the MQT rate for the fluxon in a single LJJ and for the phase-locked fluxons in a coupled LJJ stack by computing the local and nonlocal contributions. Then, we estimate the effects of the resonant cavity on the

JVQ property by computing the ground-state energy splitting. Before proceeding further, we outline the main results. (i) The potential barrier for a fluxon in the metastable state is not affected by increasing either the junction-cavity interaction or the resonant frequency of the cavity EM mode. (ii) The nonlocal contribution to the tunneling rate due to the junction-cavity interaction is negligible in the weak-coupling regime. (iii) Due to potential renormalization induced by the junction-cavity interaction, the potential barrier height for the fluxon trapped in a double-well potential is reduced. This reduction leads to an increase in the ground-state energy splitting for the JVQ with increasing junction-cavity coupling and resonant frequency.

The outline of the remainder of the paper is as follows. In Sec. II, we describe the LJJ-cavity system by using a set of two perturbed sine-Gordon equations. In Sec. III, the effects of the resonant cavity on the fluxon tunneling rate from the metastable state in a LJJ are discussed. In Sec. IV, we discuss MQT of phase-locked fluxons from the metastable state in a vertical stack of two coupled LJJ's. In Sec. V, the effects of interaction between the LJJ and a single mode in a high- $Q_c$  cavity on the JVQ are estimated by computing the ground-state energy splitting. Finally, we summarize the results and conclude in Sec. VI.

## II. COUPLED LONG JOSEPHSON JUNCTIONS IN A RESONANT CAVITY

To examine (i) one-fluxon tunneling in a single LJJ, (ii) phase-locked two-fluxon tunneling in a stack of two coupled LJJ's, and (iii) the ground-state energy splitting in the JVQ, we start with coupled perturbed sine-Gordon equations<sup>14</sup> to describe two LJJ's that interact with the resonant cavity,<sup>12</sup>

$$\frac{\partial^2}{\partial x^2}(\varphi_1 - \mathcal{S}\varphi_2) - \frac{\partial^2 \varphi_1}{\partial t^2} - \sin \varphi_1 = \mathcal{F}_1, \quad (1)$$

$$\frac{\partial^2}{\partial x^2}(\varphi_2 - \mathcal{S}\varphi_1) - \frac{\partial^2 \varphi_2}{\partial t^2} - \sin \varphi_2 = \mathcal{F}_2, \quad (2)$$

where  $x$  and  $t$  are the dimensionless coordinates in units of  $\lambda_J \gamma^{-1}(\mathcal{S})$  and  $\omega_p^{-1}$ , respectively. Here  $\gamma^{-1}(\mathcal{S}) = \sqrt{1 - \mathcal{S}^2}$  and  $\omega_p$  denotes the plasma frequency. The dynamic variable  $\varphi_i$  represents the difference between the phase  $\phi$  of the superconductor order parameter for the two superconductor ( $\mathcal{S}$ ) layers  $i$  and  $i - 1$  (i.e.,  $\varphi_i = \phi_i - \phi_{i-1}$ ). The strength of magnetic induction coupling between two LJJ's is denoted by  $\mathcal{S}$ . Here we set  $\hbar = k_B = c = 1$  for convenience. The perturbation term  $\mathcal{F}$  for each LJJ, which is given by

$$\mathcal{F}_i = \beta \frac{\partial \varphi_i}{\partial t} + f_i - g_E \frac{d^2 q_r}{dt^2} - \epsilon_i \delta(x - x_i^o) \sin \varphi_i, \quad (3)$$

accounts for the contribution from dissipation ( $\beta$ ), bias current ( $f = J^B/J_c$ ), resonant cavity ( $g_E$ ), and microresistors [ $\epsilon = (J_c - J_c')l_b/J_c \lambda_J$ ]. Here  $x_i^o$ ,  $J^B$ ,  $J_c$ ,  $J_c'$ ,  $l_b$  ( $\ll \lambda_J$ ), and  $\lambda_J$  denote the position of microresistors in the insulator layer of the  $i$ th junction, the bias current density, the critical current density, the modified current density, the length of the LJJ in which  $J_c$  is modified, and the Josephson length, respectively. We note that dissipation, bias currents, resonant cavity, and microresistors on the phase dynamics lead to different effects.

We account for the perturbation contribution due to resonant cavity by following Tornes and Stroud<sup>12</sup> and by assuming that the cavity supports a single harmonic-oscillator mode, which may be represented by the *displacement* variable  $q_r$  as

$$\frac{d^2 q_r}{dt^2} + \frac{\omega_r}{Q_c} \frac{dq_r}{dt} + \omega_r^2 q_r = \frac{g_E \gamma(\mathcal{S})}{M_{\text{osc}}} \int dx \frac{\partial^2}{\partial t^2} (\varphi_1 + \varphi_2). \quad (4)$$

Here  $\omega_r$ ,  $Q_c$ , and  $M_{\text{osc}}$  are the dimensionless oscillator frequency in units of  $\omega_p$ , the cavity quality factor, and the "mass" of the oscillator mode, respectively. For simplicity, we neglect the second term on the left-hand side of Eq. (4) by assuming that the cavity is nondissipative (i.e., high- $Q_c$  cavity). Also, we assume that the cavity electric field  $\mathbf{E}$  is uniform within the junction by considering the spatially uniform junction-cavity coupling  $g_E$  of

$$g_E = -\frac{\epsilon_d}{2e} \sqrt{\frac{M_{\text{osc}}}{4\pi}} \mathbf{E} \cdot \hat{\mathbf{z}}, \quad (5)$$

where  $\epsilon_d$  is the dielectric constant. As we will discuss later, the position-independent coupling  $g_E$  does not change the fluxon motion directly but yields potential renormalization when a microresistor is present.

To estimate the effects of interaction between the LJJ and the resonant cavity analytically, we consider the weak perturbation  $\mathcal{F}$  limit. As each perturbation term in Eq. (3) is small and does not change the form of the kink solution within the lowest-order approximation,<sup>28</sup> we describe the fluxon motion in terms of the center coordinate  $q(t)$ . In the absence of both the perturbation terms ( $\mathcal{F} = 0$ ) and the magnetic induction effect ( $\mathcal{S} = 0$ ), the fluxon solution to Eq. (1) is given by

$$\varphi_i(x, t) \approx 4 \tan^{-1} [e^{\gamma(v_i)[x - q_i(t)]}], \quad (6)$$

in the nonrelativistic limit (i.e.,  $v \ll 1$ ). Here  $q_i(t) = v_i t$  denotes the center coordinate for the fluxon, and  $v$  is the fluxon speed in units of Swihart velocity. Equation (6) represents the propagation of a nonlinear wave as a ballistic particle. The perturbation contributions of  $\mathcal{F}$  only affect the dynamics of a fluxon expressed in the  $q$  coordinate.

We now describe the fluxon phase dynamics in the coupled LJJ using the center coordinate  $q_i$  representation. The energy of the fluxon may be seen easily from the Euclidean Lagrangian (i.e.,  $\tau = it$ ),

$$\mathcal{L} = \mathcal{L}_o + \mathcal{L}_{\text{mag}} + \mathcal{L}_{\text{pert}} + \mathcal{L}_{\text{osc}} + \mathcal{L}_{\text{coup}}. \quad (7)$$

The first three terms for  $\mathcal{L}$  in Eq. (7) describe the LJJ contributions, while the remaining two terms arise from the resonant cavity. First, we discuss the LJJ contributions to Lagrangian  $\mathcal{L}$ . The unperturbed part of the LJJ is described by the Lagrangian  $\mathcal{L}_o$  given by

$$\mathcal{L}_o = \sum_i \int \frac{dx}{2} \left[ \left( \frac{\partial \varphi_i}{\partial \tau} \right)^2 + \left( \frac{\partial \varphi_i}{\partial x} \right)^2 + 2(1 - \cos \varphi_i) \right]. \quad (8)$$

The Lagrangian contribution from the magnetic induction effect,  $\mathcal{L}_{\text{mag}}$ , is given by

$$\mathcal{L}_{\text{mag}} = \mathcal{S} \int dx \left( \frac{\partial \varphi_1}{\partial x} \right) \left( \frac{\partial \varphi_2}{\partial x} \right). \quad (9)$$

We note that  $\mathcal{L}_{\text{mag}}$  accounts for the interaction energy  $E_{\text{int}}$  between two LJJ's due to the magnetic induction effect. The perturbation contribution to the Lagrangian,  $\mathcal{L}_{\text{pert}} = \mathcal{L}_{\text{nd}} + \mathcal{L}_{\text{d}}$ , is expressed as the sum of two terms: (i) the nondissipative ( $\mathcal{L}_{\text{nd}}$ ) and (ii) the dissipative ( $\mathcal{L}_{\text{d}}$ ) part. The nondissipative contribution comes from the bias currents and microresistors. The nondissipative Lagrangian  $\mathcal{L}_{\text{nd}}$  is expressed as the sum of the contributions from the bias current ( $\mathcal{L}_{\text{bias}}$ ) and microresistors ( $\mathcal{L}_{\text{pin}}$ ) (i.e.,  $\mathcal{L}_{\text{nd}} = \mathcal{L}_{\text{bias}} + \mathcal{L}_{\text{pin}}$ ). The bias current contribution  $\mathcal{L}_{\text{bias}}$  is given by

$$\mathcal{L}_{\text{bias}} = \sum_i \int dx f_i \varphi_i, \quad (10)$$

and the inhomogeneity contribution due to microresistors  $\mathcal{L}_{\text{pin}}$  is given by

$$\mathcal{L}_{\text{pin}} = \sum_i \int dx \epsilon_i \delta(x - x_i^o) (1 - \cos \varphi_i). \quad (11)$$

We note that  $\mathcal{L}_{\text{pin}}$  accounts for the fluxon pinning energy  $E_{\text{pin}}$ . These nondissipative contributions provide the bare fluxon potential  $V(q)$ . On the other hand, the dissipative Lagrangian  $\mathcal{L}_{\text{d}}$  accounts for the interaction between the fluxon and the environment. The effects of this contribution may be described<sup>29</sup> by following Caldeira and Leggett and by representing the environment as a heat bath. The heat bath is represented as harmonic oscillators with generalized momenta  $P_i$  and coordinates  $Q_i$ . The dissipation Lagrangian  $\mathcal{L}_{\text{d}}$  which accounts for the coupling between the phase ( $\varphi$ ) and oscillator ( $Q_i$ ) variables is given by

$$\mathcal{L}_{\text{d}} = \int dx \sum_i \left[ \frac{P_i^2}{2m_i} + \frac{m_i \omega_i^2}{2} \left( Q_i - \frac{c_i \varphi}{m_i \omega_i^2} \right)^2 \right]. \quad (12)$$

Here, the spectral function  $J_\beta(\omega)$ ,

$$J_\beta(\omega) = \frac{\pi}{2} \sum_i \frac{c_i^2}{m_i \omega_i^2} \delta(\omega - \omega_i) = \beta \omega, \quad (13)$$

is used to reproduce the dissipation effects ( $\beta$ ) in Eq. (3). The effects of dissipation on a two-state system have been studied extensively by using the spin-boson model.<sup>30</sup> In the adiabatic approximation, the energy splitting for the two-state system is known to be reduced<sup>30</sup> in the dissipative environment. However, this result does not<sup>29</sup> imply that the effects of the interaction between the two-state system and a single oscillator, which represents either a phonon or quantized radiation field, on the energy splitting are similar. In our discussion later in the paper, we neglect the dissipation effects by setting  $\beta = 0$  since these effects are small at low temperatures, and we focus on the effects due to a resonant cavity.

We now discuss the high- $Q_c$  resonant cavity contribution to the Lagrangian  $\mathcal{L}$  of Eq. (7). The resonant cavity is modeled by using the Lagrangian for a single harmonic oscillator, which represents a single EM-mode supported by the cavity. The Lagrangian for this single mode oscillator  $\mathcal{L}_{\text{osc}}$  is written as

$$\mathcal{L}_{\text{osc}} = \frac{M_{\text{osc}}}{2} \left( \frac{dq_r}{d\tau} \right)^2 + \frac{K}{2} q_r^2, \quad (14)$$

where  $K$  is the ‘‘spring constant’’ and  $q_r$  denotes the oscillator coordinate. We note that the oscillator frequency  $\omega_r$  in Eq. (4) is given by  $\omega_r = (K/M_{\text{osc}})^{1/2}$ . The capacitive coupling between the LJJ and the resonant cavity is described by the Lagrangian  $\mathcal{L}_{\text{coup}}$  as

$$\mathcal{L}_{\text{coup}} = -g_E \left( \frac{dq_r}{d\tau} \right) \int dx \sum_i \left( \frac{\partial \varphi_i}{\partial \tau} \right). \quad (15)$$

Here we assume that the coordinate  $q_r$  is spatially homogeneous and we focus on the effects of the uniform  $\mathbf{E}$  field in the cavity. We note that the interaction between the LJJ and the resonant cavity yields nonlocal effects similar to those from the dissipation term (i.e.,  $\beta \neq 0$ ).

We estimate MQT of the fluxon by using the usual semiclassical approach<sup>31</sup> of starting with the partition function  $\mathcal{Z}$  for the junction-cavity system,

$$\mathcal{Z} = \int \mathcal{D}[\varphi] \mathcal{D}[q_r] \exp\{-S[\varphi, q_r]\}, \quad (16)$$

where  $S[\varphi, q_r] = \int d\tau \mathcal{L}$  is the action and  $\mathcal{L}$  is the Lagrangian of Eq. (7). By noting that the shape distortion of the fluxon due to weak perturbation (i.e., small  $\mathcal{F}$ ) is negligible, we may rewrite the partition function  $\mathcal{Z}$  in terms of  $q(\tau)$  and  $q_r(\tau)$  as

$$\mathcal{Z} = \int \mathcal{D}[q] \int \mathcal{D}[q_r] e^{-S[q, q_r]}. \quad (17)$$

Also by noting that the Lagrangian  $\mathcal{L}_{\text{coup}}$  of Eq. (15), which accounts for the interaction between the LJJ and resonant cavity, is linear in both coordinates  $q_r$  and  $\varphi$ , we separate the partition function  $\mathcal{Z}$  into the resonant cavity and fluxon contribution by expressing  $\mathcal{Z} = \mathcal{Z}_{\text{res}} \mathcal{Z}_{\text{fluxon}}$ . The resonant cavity ( $\mathcal{Z}_{\text{res}}$ ) and fluxon ( $\mathcal{Z}_{\text{fluxon}}$ ) contribution to  $\mathcal{Z}$  are given, respectively, as  $\mathcal{Z}_{\text{res}} = \int \mathcal{D}[q_r(\omega_n)] \exp\{-S_{\text{res}}[q_r(\omega_n)]\}$  and  $\mathcal{Z}_{\text{fluxon}} = \int \mathcal{D}[q(\tau)] \exp\{-S_{\text{eff}}[q(\tau)]\}$ . The action for the resonant cavity contribution  $S_{\text{res}}[q_r]$  is given by

$$S_{\text{res}}[q_r] = T \sum_{\omega_n} \frac{M_{\text{osc}}}{2} (\omega_n^2 + \omega_r^2) \left[ q_{r,n} + \frac{2\pi g_E q_n \omega_n^2}{M_{\text{osc}} (\omega_n^2 + \omega_r^2)} \right] \times \left[ q_{r,-n} + \frac{2\pi g_E q_{-n} \omega_n^2}{M_{\text{osc}} (\omega_n^2 + \omega_r^2)} \right], \quad (18)$$

where  $q_{r,n} = q_r(\omega_n)$ ,  $q_n = q(\omega_n)$ ,  $\omega_n = 2\pi nT$  is the Matsubara frequency, and  $T$  is the temperature. The action for the fluxon contribution  $S_{\text{eff}}[q]$  is given by

$$S_{\text{eff}}[q] = \int d\tau \left[ \frac{M_e}{2} \sum_{i=1}^2 \dot{q}_i^2 + V(q) + \frac{\bar{g}_E^2 \omega_r^2}{1 - S^2} \left( \sum_{i=1}^2 q_i \right)^2 \right] - \frac{2\bar{g}_E^2}{1 - S^2} \int d\tau \dot{q}_1 \dot{q}_2 - \frac{\bar{g}_E^2}{1 - S^2} \int d\tau d\tau' K(\tau - \tau') \times \sum_{i=1}^2 q_i(\tau) \sum_{i=1}^2 q_i(\tau'), \quad (19)$$

where  $\dot{q}_i = dq_i/d\tau$ ,  $\bar{g}_E^2 = 2\pi^2 g_E^2 / M_{\text{osc}}$ ,  $M_e$  denotes the renormalized fluxon mass

$$M_e = M \left( 1 - \frac{1}{M} \frac{2\bar{g}_E^2}{1 - S^2} \right) \quad (20)$$

due to the spatially uniform junction-cavity interaction, and the  $M$  denotes the rest mass of the fluxon. The mass  $M_e$  accounts for the renormalization effect of both junction-cavity and magnetic induction interaction. The bare potential  $V(q) = V(q_1, q_2)$  is given<sup>32</sup> by

$$V(q) = - \sum_{i=1}^2 \left( 2\pi f_i q_i + \frac{2\epsilon_i}{\cosh^2 q_i} \right) - \frac{8S(q_1 - q_2)}{\sinh(q_1 - q_2)}. \quad (21)$$

Here, the fluxon potential  $V(q)$  includes the effects from the three contributions: (i) the potential tilting effect ( $f$ ), (ii) the pinning effect ( $\epsilon$ ), and (iii) the magnetic induction effect ( $S$ ). The third term in the large square brackets in Eq. (19) accounts for the potential renormalization due to the junction-cavity interaction. This renormalization is similar to that for the electronic tunneling process with phonon coupling.<sup>33</sup> In the later discussion, we denote  $\bar{g}_E^2$  as the strength of the junction-cavity interaction. The cavity kernel  $K(\tau - \tau')$  in the third term of Eq. (19) is given by

$$K(\tau) = \frac{\omega_r^3 \cosh(\omega_r/2T - \omega_r|\tau|)}{2 \sinh(\omega_r/2T)} \quad (22)$$

at nonzero temperature  $T$ . This term accounts for the nonlocal effect arising from the junction-cavity interaction.

After the calculation, the oscillator coordinate  $q_r$  in the partition function  $\mathcal{Z}$  of Eq. (16) is decoupled from the center coordinate  $q$ . This separation allows us to integrate out the  $q_r$  coordinate. Hence, in later discussions, we will consider the fluxon contribution  $\mathcal{Z}_{\text{fluxon}}$  to the partition function, which is described by the action  $S_{\text{eff}}$ . Using  $S_{\text{eff}}$ , we discuss how the junction-cavity interaction affects both one-fluxon and two-fluxon tunneling in LJJ's.

### III. MACROSCOPIC QUANTUM TUNNELING IN A SINGLE JUNCTION

We now examine the effects of a resonant cavity on MQT from the metastable state in a single LJJ obtained by implanting a microresistor in the insulator layer and by applying the bias current ( $J^B$ ), as shown in Fig. 1. The dimensions of the junction, compared to the Josephson length  $\lambda_J$ , are chosen so that  $L_x \gg \lambda_J$  and  $L_y \ll \lambda_J$ . These choices are made to enhance the quantum effect at low temperatures. We describe MQT of the fluxon by starting with the action  $S_{\text{eff}}^s[q]$  for the LJJ given by

$$S_{\text{eff}}^s[q] = \int d\tau \left[ \frac{M_e}{2} \dot{q}^2 + V_s(q) + \bar{g}_E^2 \omega_r^2 q^2 \right] - \bar{g}_E^2 \int d\tau d\tau' K(\tau - \tau') q(\tau) q(\tau'). \quad (23)$$

Here, the action  $S_{\text{eff}}^s[q]$  is obtained from  $S_{\text{eff}}[q]$  of Eq. (19), by setting  $S = 0$  (i.e., no magnetic induction effect),  $q_1 = q$ , and  $q_2 = 0$ . Following Caldeira and Leggett, we may simplify  $S_{\text{eff}}^s[q]$  by making a usual substitution of  $q(\tau)q(\tau') = [q^2(\tau) + q^2(\tau')]/2 - [q(\tau) - q(\tau')]^2/2$ . We note that the first two terms of this substitution cancel the potential renormalization contribution (i.e.,  $\bar{g}_E^2 \omega_r^2 q^2$  term) arising from the junction-cavity interaction. With this cancellation, the action  $S_{\text{eff}}^s[q]$  becomes similar to that for the dissipative system,<sup>29</sup> but the

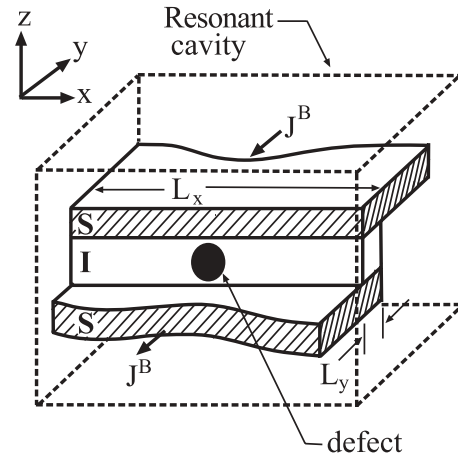


FIG. 1. A LJJ is shown schematically as an insulator ( $I$ ) layer is sandwiched between two superconductor ( $S$ ) layers.  $L_x$  and  $L_y$  denote the dimensions in the  $x$  and  $y$  direction, respectively.  $J^B$  denotes the bias current density. The filled circle represents the microresistor (i.e., pinning center) and the dashed box represents the resonant cavity.

fluxon mass is now renormalized to

$$M_e = M \left( 1 - \frac{2\bar{g}_E^2}{M} \right) \quad (24)$$

and  $\beta$  is replaced by the junction-cavity interaction strength (i.e.,  $\beta \rightarrow \bar{g}_E^2$ ). The renormalized mass  $M_e$  accounts for the effects of the uniform  $\mathbf{E}$  field in the cavity. The bare fluxon potential  $V_s(q)$  is given by

$$V_s(q) = -2\pi f q - \frac{2\epsilon}{\cosh^2 q}. \quad (25)$$

Here the bias current density  $f = f_c - \delta_f$  is measured in terms of the deviation  $\delta_f$  from the critical value  $f_c = 4\epsilon/(3\sqrt{3}\pi)$ . The potential  $V_s(q)$  may be approximated by a quadratic-cubic potential as shown schematically in Fig. 2. The cavity kernel  $K(\tau - \tau')$  of Eq. (22) describing the nonlocal effect due to the junction-cavity interaction simplifies to

$$K(\tau - \tau') = \frac{\omega_r^3}{2} e^{-\omega_r|\tau - \tau'|} \quad (26)$$

in the  $T = 0$  limit.

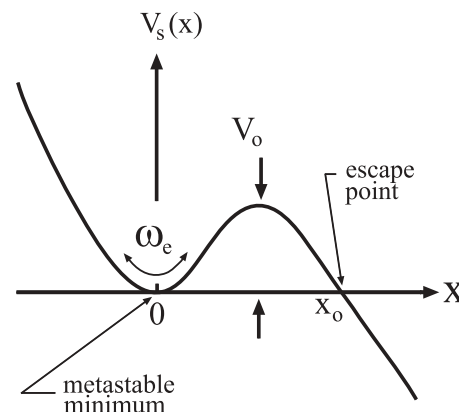


FIG. 2. The fluxon potential  $V_s$  due to both the bias current density and the microresistor in a single LJJ is schematically illustrated.



The action  $S_{\text{eff}}^s[q]$  of Eq. (23) indicates that the resonant cavity yields (i) fluxon mass renormalization and (ii) nonlocal effects. The mass renormalization modifies the oscillation frequency about the metastable point, as shown in Fig. 2. This change may be easily seen by computing the oscillation frequency  $\omega_e$  at the metastable state (i.e., local minimum) as

$$\omega_e = \left[ \frac{1}{M_e} \frac{d^2 \bar{V}_s(0)}{dx^2} \right]^{1/2} \approx \omega_o \left( 1 + \frac{\bar{g}_E^2}{M} \right), \quad (27)$$

where  $\omega_o$  is the oscillation frequency at the metastable point in the absence of the resonant cavity. The nonlocal contribution due to junction-cavity interaction is similar to that for the dissipative system, but to determine the size of this contribution more calculation is needed.

To estimate the size of these two contributions from the junction-cavity interaction, we compute the MQT rate<sup>29,34</sup> given by

$$\Gamma_{\text{cav}}(0) = \mathcal{A}_{\text{cav}}(0) e^{-\mathcal{B}_{\text{cav}}(0)} \quad (28)$$

at  $T = 0$ . Here, the prefactor  $\mathcal{A}_{\text{cav}}(0)$  is given by

$$\mathcal{A}_{\text{cav}}(0) = \sqrt{60} \omega_e \left( \frac{\mathcal{B}_{o,\text{cav}}}{2\pi} \right)^{1/2} \quad (29)$$

and the bounce exponent  $\mathcal{B}_{\text{cav}}(0) = \mathcal{B}_{o,\text{cav}} + \delta\mathcal{B}_{\text{cav}}$  includes both the local contribution  $\mathcal{B}_{o,\text{cav}}$  of

$$\mathcal{B}_{o,\text{cav}} = \int_{-\infty}^{\infty} d\tau \left[ \frac{M_e}{2} \dot{q}^2 + V_s(q) \right] \quad (30)$$

and the nonlocal contribution  $\delta\mathcal{B}_{\text{cav}}$  of

$$\delta\mathcal{B}_{\text{cav}} = \bar{g}_E^2 \int_{-\infty}^{\infty} d\tau \int_{-\infty}^{\infty} d\tau' K(\tau - \tau') [q(\tau) - q(\tau')]^2. \quad (31)$$

These two contributions,  $\mathcal{B}_{o,\text{cav}}$  and  $\delta\mathcal{B}_{\text{cav}}$ , to  $\mathcal{B}_{\text{cav}}(0)$  are evaluated explicitly to estimate their size.

The local contribution  $\mathcal{B}_{o,\text{cav}}$  may be computed easily by approximating  $V_s(q)$  of Eq. (25) as a usual quadratic-plus-cubic potential of

$$\bar{V}_s(x) = V_s(q) - V_s(q_o) \approx \frac{27V_o}{4} (\bar{x}^2 - \bar{x}^3), \quad (32)$$

where  $\bar{x} = x/x_o$ ,  $x = q - q_o$ , and  $V_o = [8\pi^3 \delta_f^3 / (\sqrt{3}\epsilon)]^{1/2}$  is the barrier potential for the fluxon. Here  $q_o$  is the position of the metastable point and  $x_o = 9\sqrt{3}M_e\omega_e^2/32\epsilon$  is the escape point as shown in Fig. 2. The evaluation of  $\mathcal{B}_{o,\text{cav}}$  yields

$$\mathcal{B}_{o,\text{cav}} = 2 \int_o^{x_o} dx [2M_e \bar{V}_s(x)]^{1/2} = \frac{36V_o}{5\omega_e}. \quad (33)$$

Using this result, we estimate the local contribution to enhancement of the tunneling rate due to the resonant cavity. The ratio of the MQT rates,  $\Gamma_{\text{cav}}(0)/\Gamma(0)$ , is given by

$$\frac{\Gamma_{\text{cav}}(0)}{\Gamma(0)} \approx 1 + \frac{\bar{g}_E^2}{2M} \left( 1 + \frac{72V_o}{5\omega_o} \right), \quad (34)$$

where  $\Gamma(0)$  is the tunneling rate in the absence of the resonant cavity (i.e.,  $\bar{g}_E^2 = 0$ ). Equation (34) indicates that the tunneling rate increases with increasing junction-cavity interaction strength  $\bar{g}_E^2$ . In Fig. 3, we plot the numerically computed ratio  $\Gamma_{\text{cav}}(0)/\Gamma(0)$  as a function of  $\bar{g}_E^2$  to illustrate its enhancement in the weak-coupling regime (i.e.,  $\bar{g}_E^2 \ll 1$ ).

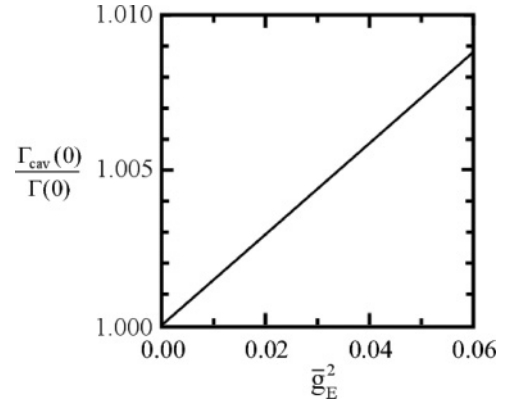


FIG. 3. The ratio of the tunneling rates  $\Gamma_{\text{cav}}(0)/\Gamma(0)$  is plotted as a function of the junction-cavity coupling strength  $\bar{g}_E^2$  to illustrate the size of enhancement.

The curve indicates that enhancement of  $\Gamma_{\text{cav}}(0)/\Gamma(0)$  is less than 1%.

The nonlocal contribution  $\delta\mathcal{B}_{\text{cav}}$  to  $\mathcal{B}_{\text{cav}}(0)$  of Eq. (28) reduces the tunneling rate  $\Gamma_{\text{cav}}(0)$ . The size of this reduction is estimated by evaluating  $\delta\mathcal{B}_{\text{cav}}$  of Eq. (31) by writing

$$\delta\mathcal{B}_{\text{cav}} = \frac{\bar{g}_E^2 \omega_r^3 x_o^2}{\omega_e^2} \int_{-\infty}^{\infty} d\bar{\tau} d\bar{\tau}' e^{-\frac{2\omega_r}{\omega_e} |\bar{\tau} - \bar{\tau}'|} [\bar{x}(\bar{\tau}) - \bar{x}(\bar{\tau}')]^2, \quad (35)$$

where  $\bar{x}(\tau) = \text{sech}^2(\omega_e \tau/2)$ . We note that  $\bar{x}(\tau)$  is the solution to the equation of motion for the quadratic-plus-cubic potential in the absence of the nonlocal effect. We evaluate Eq. (35) and obtain

$$\delta\mathcal{B}_{\text{cav}} = 2\bar{g}_E^2 \left( \frac{9\sqrt{3}M_e}{16\epsilon} \right)^2 \frac{\omega_r^5}{\sinh^2(\pi\omega_r/\omega_e)}. \quad (36)$$

The result for  $\delta\mathcal{B}_{\text{cav}}$  indicates that the nonlocal contribution increases almost linearly with  $\bar{g}_E^2$  in the weak-coupling regime and has a strong dependence on the frequency  $\omega_r$  of the cavity mode. At low cavity frequencies ( $\omega_r \ll 1$ ), the nonlocal contribution varies as  $\delta\mathcal{B}_{\text{cav}} \propto \omega_r^3$ . At high cavity frequencies ( $\omega_r \gg 1$ ), on the other hand, it varies as  $\delta\mathcal{B}_{\text{cav}} \propto \omega_r^5 \exp(-2\pi\omega_r/\omega_e)$ . To illustrate the cavity frequency dependence, we plot  $\delta\mathcal{B}_{\text{cav}}$  as a function of  $\omega_r$  for  $\bar{g}_E^2 = 0.02$  (solid line), 0.04 (dashed line), and 0.06 (dot-dashed line) in Fig. 4. The curves indicate that

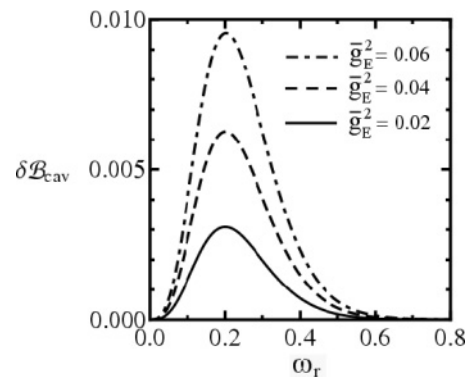


FIG. 4. The nonlocal contribution  $\delta\mathcal{B}_{\text{cav}}$  to the bounce exponent  $\mathcal{B}_{\text{cav}}(0)$  is plotted as a function of  $\omega_r$  for  $\bar{g}_E^2 = 0.02$  (solid line), 0.04 (dashed line), and 0.06 (dot-dashed line).

$\delta\mathcal{B}_{\text{cav}}$  vanishes both in the low and high cavity frequency  $\omega_r$  limits. Hence, the nonlocal effect on the tunneling rate  $\Gamma_{\text{cav}}(0)$  is negligible near these limits.

#### IV. MACROSCOPIC QUANTUM TUNNELING IN COUPLED JUNCTIONS

In this section, we estimate the effects of a resonant cavity on the tunneling rate of the phase-locked fluxons from the metastable state in two coupled LJJ's. Here the fluxons are trapped by the microresistor on each insulator (I) layer, shown schematically in Fig. 5. Earlier studies<sup>25</sup> indicate that uncorrelated one-fluxon tunneling is the dominant process in the absence of a resonant cavity. However, phase-locking between the fluxons in two LJJ's becomes enhanced in the resonant cavity. This enhancement may be seen more easily from the effective action  $S_{\text{eff}}[q]$  for the two coupled LJJ's of Eqs. (19) and (21) written in the rotated coordinates  $(q_+, q_-)$  as

$$S_{\text{eff}}[q] = \int d\tau \left[ \frac{M_e}{2} \dot{q}_+^2 + \frac{M}{2} \dot{q}_-^2 + V(\mathbf{q}) + \frac{\bar{g}_E^2 \omega_r^2}{1 - S^2} q_+^2 \right] - \frac{2\bar{g}_E^2}{1 - S^2} \int d\tau d\tau' K(\tau - \tau') q_+(\tau) q_+(\tau'), \quad (37)$$

where  $q_{\pm} = (q_1 \pm q_2)/\sqrt{2}$ . The action  $S_{\text{eff}}[q]$  indicates that the potential for the in-phase mode,  $(q_+, 0)$ , is renormalized by the junction-cavity interaction while the out-of-phase mode,  $(0, q_-)$ , is not. Also, the nonlocal contribution appears only for the motion in the  $q_+$  direction. The bare fluxon potential  $V(\mathbf{q}) = V(q_+, q_-)$  of

$$V(q_+, q_-) = -2\sqrt{2}\pi f q_+ - \frac{8\sqrt{2}S q_-}{\sinh \sqrt{2}q_-} - 2\epsilon \left[ \frac{1}{\cosh^2 \left( \frac{q_+ + q_-}{\sqrt{2}} \right)} + \frac{1}{\cosh^2 \left( \frac{q_+ - q_-}{\sqrt{2}} \right)} \right] \quad (38)$$

for  $f_1 = f_2 = f$  and  $\epsilon_1 = \epsilon_2 = \epsilon$  indicates that the one-dimensional potential along the  $(q_+, 0)$  direction [i.e.,  $V(q_+, 0)$ ]

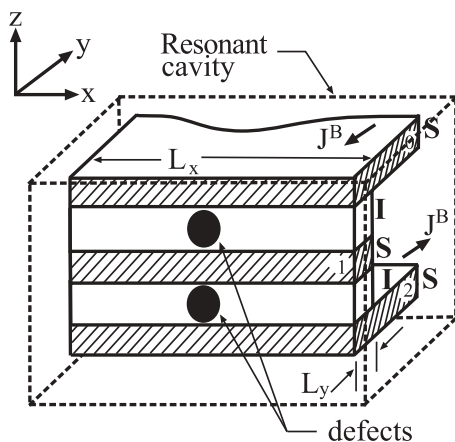


FIG. 5. Two LJJ's with a vertical column of two microresistors is shown schematically.  $L_x$  and  $L_y$  denote the dimensions in the  $x$  and  $y$  directions, respectively.  $J^B$  denotes the bias current density. The filled circles represent the microresistors.

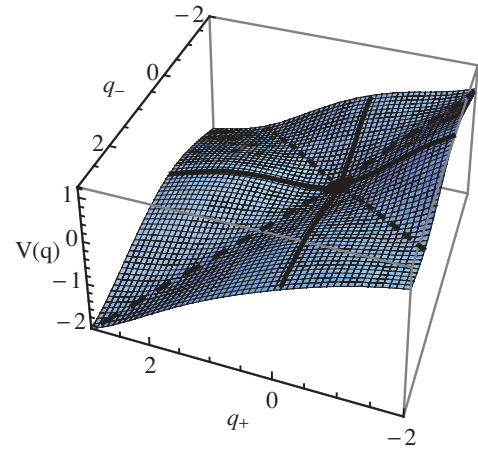


FIG. 6. (Color online) The potential  $V_Q(q_+, q_-)$  surface is plotted for  $\epsilon = 0.269$  and  $S = -0.05$ . The filled circle represents the position of the metastable state. The dashed and solid lines denote the most probable escape paths (MPEP's) for one-fluxon and two-fluxon tunneling, respectively.

corresponding to the in-phase mode becomes identical to  $V_s(q)$  of Eq. (25) under the transformation of  $2f \rightarrow f$ ,  $2\epsilon \rightarrow \epsilon$ , and  $q_+/\sqrt{2} \rightarrow q$ . This similarity reflects that the phase-locked fluxons moving in the  $(q_+, 0)$  direction (i.e.,  $q_1 = q_2$ ) behave as a single fluxon. However, the one-dimensional potential for the out-of-phase mode [i.e.,  $V(0, q_-)$  or along the  $(0, q_-)$  direction] behaves as a potential well near the metastable point  $\mathbf{q}^o = (q_+^o, q_-^o)$ , determined from the condition  $[\partial V(\mathbf{q})/\partial q_+]_{q_-} = [\partial V(\mathbf{q})/\partial q_-]_{q_+} = 0$ .

To illustrate these phase-locking modes, we plot the potential  $V(q_+, q_-)$  in Fig. 6 for  $f = 0.06$ ,  $\epsilon = 0.269$ , and  $S = -0.05$ . Here, the values for  $\epsilon$  and  $S$  are chosen so that when a vertical stack<sup>35</sup> of two interacting JVQ's is fabricated using coupled LJJ's and microresistors, only one quantum state is bound on each side of the double-well potential. The metastable point  $\mathbf{q}^o$  is denoted by the solid circle. The solid lines indicate that the potential is metastable for the in-phase mode [i.e., along the  $(q_+, 0)$  direction], but it behaves as a well for the out-of-phase mode [i.e., along the  $(0, q_-)$  direction]. These curves show that tunneling of the in-phase mode from the metastable state is more favorable than that for the out-of-phase mode.

The tunneling rate  $\Gamma_{\text{cav}}(0)$  from  $\mathbf{q}^o$  can be estimated by summing over the contribution from all paths of escape, but the dominant contribution comes from the MPEP in which  $S_{\text{eff}}$  is the minimum.<sup>36</sup> For the physical parameters chosen in Fig. 6, the MPEP's correspond to one-fluxon tunneling, indicated by the dashed lines. The MPEP's are determined by the two competing energies: (i) the pinning energy ( $\mathcal{E}_{\text{pin}} = |E_{\text{pin}}|$ ) and (ii) the magnetic induction interaction energy ( $\mathcal{E}_{\text{int}} = |E_{\text{int}}|$ ). When  $\mathcal{E}_{\text{int}} \gg \mathcal{E}_{\text{pin}}$ , the fluxons are not pinned at the microresistor sites but maintain a large separation distance.<sup>32</sup> However, when  $\mathcal{E}_{\text{int}} \ll \mathcal{E}_{\text{pin}}$ , the one-fluxon tunneling processes are favored over the two-fluxon tunneling processes.

We now estimate the two-fluxon tunneling rate for the in-phase mode. We simplify the calculation by using the similarity between the tunneling of the in-phase mode and the one-fluxon tunneling process discussed in Sec. III. When

the bias current  $f$  is less than the critical value  $f_c$  [i.e.,  $f = f_c - \delta_f$  with  $0 < \delta_f \ll f_c = 4\epsilon/(3\sqrt{3}\pi)$ ], the potential along the path  $(q_+, 0)$  has the metastable state, as illustrated in Fig. 2. The potential  $V(q_+, 0)$  may be approximated as the quadratic-plus-cubic form of

$$V(\bar{q}_+, 0) \approx \frac{27V_o^t}{4}(\bar{q}_+^2 - \bar{q}_+^3), \quad (39)$$

where  $\bar{q}_+ = (q_+ - q_+^o)/q_+^e$ ,  $q_+^e$  is the escape point, and  $V_o^t = 2[d^2V(q_+^o, 0)/dq_+^2]^3/3[d^3V(q_+^o, 0)/dq_+^3]^2$  denotes the potential barrier height for two-fluxon tunneling. We note that  $q_+^e$  is similar to  $x_o$  in Fig. 2. Also, similar to the single LJJ, the semiclassically estimated two-fluxon tunneling rate of  $\Gamma_{\text{cav}}^t(0) = \mathcal{A}_{\text{cav}}^t \exp[\mathcal{B}_{\text{cav}}^t(0)]$  at  $T = 0$  depends on both the barrier height and oscillation frequency. The factor  $\mathcal{A}_{\text{cav}}^t(0)$  and bounce exponent  $\mathcal{B}_{\text{cav}}^t(0)$  are calculated in the same way as in Sec. III. The factor  $\mathcal{A}_{\text{cav}}^t(0)$  is given by

$$\mathcal{A}_{\text{cav}}^t(0) \approx \sqrt{60}\omega_e \left( \frac{\mathcal{B}_{o,\text{cav}}^t}{2\pi} \right)^{1/2}. \quad (40)$$

The local and nonlocal contributions to the bounce exponents  $\mathcal{B}_{\text{cav}}^t(0) = \mathcal{B}_{o,\text{cav}}^t + \delta\mathcal{B}_{\text{cav}}^t$  are given by

$$\mathcal{B}_{o,\text{cav}}^t = 2 \int_0^{q_+^e - q_+^o} dq_+ \sqrt{2M_e V(q_+, 0)} \approx \frac{36V_o^t}{5\omega_e} \quad (41)$$

and

$$\delta\mathcal{B}_{\text{cav}}^t \approx \frac{2\bar{g}_E^2}{1 - S^2} \left( \frac{9\sqrt{3}M_e}{16\epsilon} \right)^2 \frac{\omega_r^5}{\sinh^2(\pi\omega_r/\omega_e)}, \quad (42)$$

respectively. The result indicates that the two-fluxon tunneling rate  $\Gamma_{\text{cav}}^t(0)$  in the cavity is enhanced from that  $\Gamma^t(0)$  in its absence. Neglecting the nonlocal contribution, we may write the ratio  $\Gamma_{\text{cav}}^t(0)/\Gamma^t(0)$  as

$$\frac{\Gamma_{\text{cav}}^t(0)}{\Gamma^t(0)} \approx 1 + \frac{\bar{g}_E^2}{2M(1 - S^2)} \left( 1 + \frac{72}{5} \frac{V_o^t}{\omega_o} \right). \quad (43)$$

This enhancement is similar to the tunneling process discussed in Sec. III. The estimated value of  $\Gamma^t(0)$  for the Nb-Al<sub>2</sub>O<sub>x</sub>-Nb-Al<sub>2</sub>O<sub>x</sub>-Nb junction is  $8.5 \times 10^9 \text{ s}^{-1}$ . This value is obtained by using the experimental value<sup>14,16</sup> of  $J_c \sim 2 \times 10^6 \text{ A/m}^2$ ,  $\lambda_L \sim 90 \text{ nm}$ ,  $\lambda_J \sim 25 \mu\text{m}$ , and  $\omega_p \sim 90 \text{ GHz}$ . Also, we chose  $L_y \sim 0.2 \mu\text{m}$  to enhance the quantum effect and used the experimentally accessible values<sup>23</sup> of  $\epsilon = 0.269$ ,  $S = -0.05$ , and  $\delta_f \sim 5 \times 10^{-4}$ . On the other hand, the potential  $V(q_+, q_-)$  along the  $(q_+, 0)$  direction indicates that the two-fluxon tunneling rate  $\Gamma_{\text{cav}}^t(0)$  is suppressed from the one-fluxon tunneling rate  $\Gamma_{\text{cav}}^o(0)$  along either the  $q_+ = q_-$  or  $q_+ = -q_-$  direction. This reduction in the tunneling rate is given by

$$\frac{\Gamma_{\text{cav}}^t(0)}{\Gamma_{\text{cav}}^o(0)} \approx \alpha_o \sqrt{\frac{V_o^t}{V_o^o}} e^{-\frac{36(V_o^t - \alpha_o^2 V_o^o)}{5\omega_o}} \times \left[ 1 + \frac{36\bar{g}_E^2(V_o^t - \alpha_o^2 V_o^o)}{5\omega_o M(1 - S^2)} \right], \quad (44)$$

where  $\alpha_o = \{[d^2V(q_+^o, 0)/dq_+^2]/[d^2V(q^o, 0)/dq^2]\}^{1/4}$  is a constant of order unity,  $V_o^o = 2[d^2V(q^o, 0)/dq^2]^3/3[d^3V(q^o, 0)/dq^3]^2$  is the one-fluxon tunneling potential barrier height,  $V(q, 0)$  is the fluxon potential of Eq. (21)

along the  $q_+ = q_-$  direction, and  $q^o$  denotes the position of the metastable point for one-fluxon tunneling, given by the condition that  $dV(q^o, 0)/dq = 0$ . The ratio  $\Gamma_{\text{cav}}^t(0)/\Gamma_{\text{cav}}^o(0) \ll 1$  for the potential surface in Fig. 6 reflects that  $V_o^t \gg V_o^o$ .

## V. JOSEPHSON VORTEX QUBIT IN A RESONANT CAVITY

We now examine the effects of a high- $Q_c$  resonant cavity on JVQ. The JVQ may be fabricated by using two closely implanted microresistors in the insulator layer of the linear LJJ, as shown in Fig. 7. As earlier studies<sup>2-4</sup> indicate, MQT of a fluxon between the spatially separated minima of a double-well potential leads to splitting of the degenerate ground-state energy.<sup>37,38</sup> In this section, we estimate the effects of junction-cavity interaction on this energy splitting.

The interaction between the LJJ and the resonant cavity yields (i) a fluxon potential renormalization and (ii) a nonlocal contribution to the action. The effects of these contributions on the energy splitting may be estimated by starting with the action  $S_{\text{eff}}^Q$  for the JVQ given by

$$S_{\text{eff}}^Q[q] = \int d\tau \left[ \frac{M_e}{2} \dot{q}^2 + V_Q(q) \right] - 2\bar{g}_E^2 \int d\tau d\tau' K(\tau - \tau') q(\tau) q(\tau'). \quad (45)$$

Without loss of generality, we obtain the potential function  $V_Q(q)$  from the double-well potential  $V(q)$  of

$$V(q) = \bar{g}_E^2 \omega_r^2 q^2 - \frac{2\epsilon}{\cosh^2(q - \ell/2)} - \frac{2\epsilon}{\cosh^2(q + \ell/2)}, \quad (46)$$

where  $\ell$  denotes the separation distance between the two microresistors. Here, we have added a constant energy  $E_Q$  term to  $V(q)$  [i.e.,  $V_Q(q) = V(q) + E_Q$ ] so that  $V_Q(q)$  vanishes at the potential minima. Here, the potential  $V_Q(q)$  may be characterized by the position of the two minima and the potential barrier height. In the discussion later, we do not make

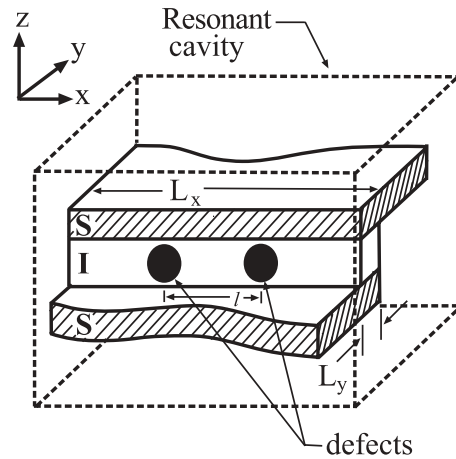


FIG. 7. A LJJ with two microresistors, representing a Josephson vortex qubit, in a resonant cavity is shown schematically. The separation distance between the microresistors is denoted by  $\ell$ . The filled circles and dashed box represent the microresistors and the resonant cavity, respectively.

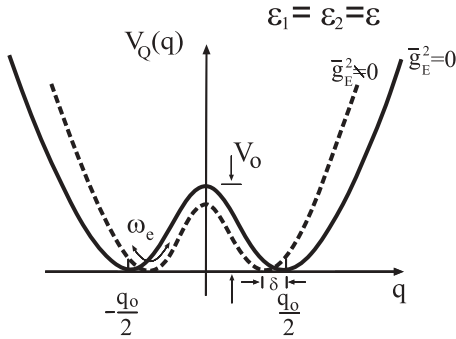


FIG. 8. A schematic diagram of a double-well potential  $V_Q(q)$  due to the two microresistors in the insulator layer of the LJJ is shown to illustrate the renormalization of  $V_Q(q)$ . The solid and dashed lines represent the potential  $V_Q(q)$  in the absence and in the presence of the resonant cavity, respectively.

the usual substitution of  $q(\tau)q(\tau') = [q^2(\tau) + q^2(\tau')]/2 - [q(\tau) - q(\tau')]^2/2$  used in Sec. III. This approach allows us to elucidate the origin of the changes in the energy splitting due to the junction-cavity interaction.

In the absence of the resonant cavity (i.e.,  $\bar{g}_E^2 = 0$ ), the double-well structure for  $V_Q(q)$  with the separation distance  $\ell > \ell_o \approx 1.317$  is shown schematically in Fig. 8 as the solid line. The two potential minima are located at  $q = \pm q_o/2$ , where  $q_o$  is determined from

$$\cosh q_o = \frac{\sinh^2 \ell - 1}{\cosh \ell}. \quad (47)$$

The energy shift  $E_Q$ , representing a constant of motion, is given by

$$E_Q = -2\epsilon \frac{\cosh^2 \ell}{\cosh^2 \ell - 1}. \quad (48)$$

Also, the potential barrier height  $V_o$  between the two minima (i.e.,  $q = \pm q_o/2$ ) is given by

$$V_o = 2\epsilon \left( \frac{\cosh \ell - 2}{\sinh \ell} \right)^2. \quad (49)$$

We note that these quantities change in the resonant cavity, as shown schematically by the dashed line in Fig. 8.

In the resonant cavity (i.e.,  $\bar{g}_E^2 \neq 0$ ), on the other hand, the JVQ potential  $V_Q(q)$  acquires an additional  $\bar{g}_E^2 \omega_r^2 q^2$  term in Eq. (46). This term arises from the coupling between the oscillator coordinate  $q_r$  and the center coordinate  $q$  in the coupling Lagrangian  $\mathcal{L}_{\text{coup}}$  of Eq. (15) and accounts for potential renormalization. The main renormalization effects are the following: (i) the barrier potential height is reduced, (ii) the positions of the potential minima become closer together, and (iii) the oscillation frequency at the potential minima is modified. These effects become amplified with increasing junction-cavity interaction strength ( $\bar{g}_E^2$ ) and resonant frequency ( $\omega_r$ ).

The effects of the junction-cavity interaction on the potential barrier height  $V_{o,\text{cav}}$  may be estimated straightforwardly. In Fig. 9, we plot the numerically computed ratio  $V_{o,\text{cav}}/V_o$  as a function of  $\bar{g}_E^2$  to illustrate the dependence on the junction-cavity interaction. The curves for  $\omega_r = 0.50$  (dot-dashed line), 0.70 (dashed line), and 0.90 (solid line) indicate that the barrier

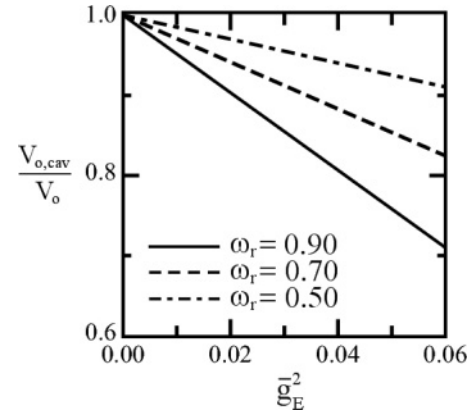


FIG. 9. The ratio of the potential barrier height  $V_{o,\text{cav}}/V_o$  is plotted as a function of the junction-cavity coupling strength  $\bar{g}_E^2$  for  $\omega_r = 0.50$  (dot-dashed line), 0.70 (dashed line), and 0.90 (solid line) to illustrate the suppression in the cavity.

potential height decreases with increasing  $\bar{g}_E^2$  and  $\omega_r$ . Also, the curves indicate that the ratio decreases linearly in the weak-coupling regime. To leading order in  $\bar{g}_E^2$ , the potential barrier height  $V_{o,\text{cav}}$  estimated from the renormalized potential  $V(q)$  of Eq. (46) is given by

$$V_{o,\text{cav}} \cong V_o - \bar{g}_E^2 \omega_r^2 q_o^2. \quad (50)$$

This decrease in the potential barrier height leads to the increase in the ground-state energy splitting.

Another important effect of the resonant cavity is the shift  $\delta_o$  in the positions of the potential minima. As the potential barrier height is reduced, the positions of the potential minima are closer together. The shift  $\delta_o$  from the initial position of  $q = \pm q_o/2$  is given by

$$\delta_o = \frac{\bar{g}_E^2 q_o \omega_r^2 \cosh^2 \ell \tanh^2 \ell}{\epsilon \cosh 2\ell - 7}. \quad (51)$$

Here, we obtained  $\delta_o$  by imposing the condition  $[dV(q)/dq]_{q=(q_o/2)_{\pm}} = 0$ , where  $(q_o/2)_{\pm} = \pm[(q_o/2) - \delta_o]$  denotes the new potential minima. This shift  $\delta_o$  modifies the constant of motion  $E_Q$ . The new value for  $E_Q$  may be obtained from the condition  $[dq(\tau)/d\tau]_{(q_o/2)_{\pm}} = 0$ , noting that the fluxon is initially located at the bottom of either side of the double-well potential so that  $V_Q[(q_o/2)_{\pm}] = 0$ . We plot the numerically computed shift  $\delta_o$  as a function of  $\bar{g}_E^2$  in Fig. 10 for  $\omega_r = 0.50$  (dot-dashed line), 0.70 (dashed line), and 0.90 (solid line) to illustrate the amount of this shift in the weak-coupling regime. The curves indicate that  $\delta_o$  increases with  $\bar{g}_E^2$  and with  $\omega_r$ , reflecting potential renormalization.

The resonant cavity also modifies the oscillation frequency  $\omega_e$  at the potential minima. The modified frequency  $\omega_e$  is given by

$$\omega_e \approx \omega_o \left\{ 1 + \frac{\bar{g}_E^2}{M} \left[ 1 + \frac{\omega_r^2}{\omega_o^2} (1 - \Upsilon) \right] \right\}, \quad (52)$$

where  $\omega_o$  is the frequency in the absence of the resonant cavity and  $\Upsilon = 6q_o \sinh 2q_o \tanh \ell / \epsilon (\cosh^2 \ell - 4) \sinh^2 \ell$ .

We now combine these effects and estimate the ground-state energy splitting<sup>37</sup>  $\Delta_{\text{cav}}$  by using the action  $S_{\text{eff}}^Q[q]$  of Eq. (45) and by using the standard method of summing



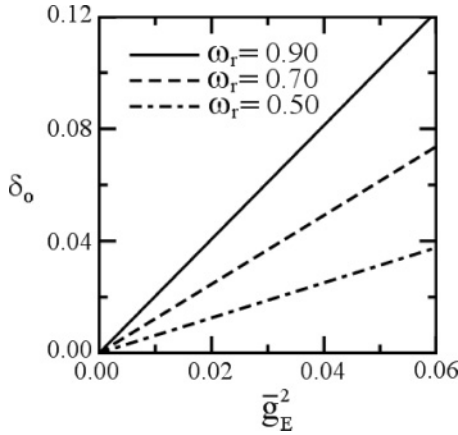


FIG. 10. The shift  $\delta_o$  in the positions of the potential minima is plotted as a function of the junction-cavity coupling strength  $\bar{g}_E^2$  for  $\omega_r = 0.50$  (dot-dashed line), 0.70 (dashed line), and 0.90 (solid line).

over the “instanton” trajectories.<sup>39</sup> By following Weiss and co-workers,<sup>40</sup> we compute the one-bounce contribution to the partition function  $\mathcal{Z}_{\text{fluxon}}$ , assuming that the fluxon is initially pinned at one of the potential minima. We write the partition function as

$$\mathcal{Z}_{\text{fluxon}} = \sum_{i=0}^{\infty} \mathcal{Z}_i, \quad (53)$$

where  $\mathcal{Z}_i$  denotes the  $i$ -bounce contribution. Here the bounce is an instanton–anti-instanton pair. To estimate  $\Delta_{\text{cav}}$ , we compute both the saddle-point ( $\mathcal{Z}_0$ ) and the one-bounce ( $\mathcal{Z}_1$ ) contribution to  $\mathcal{Z}_{\text{fluxon}}$  by noting that  $\mathcal{Z}_1$  may be expressed as

$$\mathcal{Z}_1 = \frac{\mathcal{Z}_0}{2\pi} \left( \frac{\Delta_{\text{cav}}\theta}{2} \right)^2, \quad (54)$$

where  $\theta = 1/T$ . For the contribution  $\mathcal{Z}_0$ , we assume that the fluxon is initially confined at  $q = (q_o/2)_-$  and obtain

$$\mathcal{Z}_0 = N \left( \prod_{n=0}^{\infty} \lambda_n^o \right)^{-1/2}, \quad (55)$$

where the eigenvalues  $\lambda_n^o$  are determined from

$$\left[ -M_e \partial_\tau^2 + V_Q'' \left( -\frac{q_o}{2} + \delta \right) \right] q_n^o(\tau) + 4\pi \bar{g}_E^2 \int_{-\theta/2}^{\theta/2} K(\tau - \tau') q_n^o(\tau') = \lambda_n^o q_n^o(\tau). \quad (56)$$

Here  $\partial_\tau^2 = \partial^2/\partial\tau^2$ ,  $V_Q''(q) = \partial^2 V_Q(q)/\partial q^2$ , and the cavity kernel  $K(\tau - \tau') = (\omega_r^3/2) \exp[-\omega_r |\tau - \tau'|]$  accounts for the nonlocal effect.

For the one-bounce contribution  $\mathcal{Z}_1$  to  $\mathcal{Z}_{\text{fluxon}}$ , we separate the center coordinate  $q(\tau)$  into two parts as

$$q(\tau) = \bar{q}(\tau) + \sum_{n=0}^{\infty} c_n q_n(\tau), \quad (57)$$

where  $\bar{q}(\tau)$  describes a bouncelike trajectory and the remaining terms describe the arbitrary paths about this bouncelike

trajectory. This separation of  $q(\tau)$  may be used to write the action  $S_{\text{eff}}^Q[q]$  as

$$S_{\text{eff}}^Q[q(\tau)] = S_{B,1}^{\text{cav}}[\bar{q}(\tau)] + \sum_{n=0}^{\infty} \frac{1}{2} \lambda_n c_n^2. \quad (58)$$

Here  $S_{B,1}^{\text{cav}}$  accounts for the one-bounce-like trajectory in the resonant cavity. We choose  $q_n(\tau)$  of Eq. (57) so that the eigenfunctions of the second variational derivative of  $S_{\text{eff}}^Q[q]$  at  $\bar{q}$  and the eigenvalues  $\lambda_n$  are determined from

$$\left[ -M_e \partial_\tau^2 + V_Q''(\bar{q}) \right] q_n(\tau) + 4\pi \bar{g}_E^2 \int_{-\theta/2}^{\theta/2} K(\tau - \tau') q_n(\tau') = \lambda_n q_n(\tau). \quad (59)$$

We note that the first two eigenvalues,  $\lambda_0$  and  $\lambda_1$ , need to be separated from the rest because  $\lambda_0 \leq 0$  and  $\lambda_1 = 0$  while the other eigenvalues are positive. The one-bounce contribution ( $\mathcal{Z}_1$ ) may be expressed as

$$\mathcal{Z}_1 = N \int \prod_{n=0}^{\infty} \frac{dc_n}{\sqrt{2\pi}} e^{-\left( S_{B,1}^{\text{cav}} + \frac{1}{2} \sum_{n=0}^{\infty} \lambda_n c_n^2 \right)}, \quad (60)$$

where  $N$  is a normalization constant. With the separation of the first two eigenvalues (i.e.,  $\lambda_0 \leq 0$  and  $\lambda_1 = 0$ ) from the others, we write the one-bounce contribution to the partition function as

$$\mathcal{Z}_1 \approx \frac{\mathcal{Z}_0 \theta}{2\pi} \left[ \int_0^\theta d\tau_1 e^{-S_{B,1}^{\text{cav}}(\tau_1)} \right] \left[ \frac{\prod_{n=0}^{\infty} \lambda_n^o}{\prod_{n=2}^{\infty} \lambda_n} \right]^{1/2} \times \left[ \int_{-\theta/2}^{\theta/2} d\tau \left( \frac{d\bar{q}}{d\tau} \right)^2 \right]^{1/2} \left[ \int_{-\theta/2}^{\theta/2} d\tau' \left( \frac{d\bar{q}}{d\tau'} \right)^2 \right]^{1/2}. \quad (61)$$

We now need to evaluate  $\mathcal{Z}_1$  of Eq. (61) to estimate  $\Delta_{\text{cav}}$ . Using Eq. (54), we write the ground-state energy splitting  $\Delta_{\text{cav}}$  as

$$\Delta_{\text{cav}} = \frac{2\omega_e}{\sqrt{\pi}} \left( R_{\text{cav}} L_{\text{cav}} e^{-S_{B,1}^{\text{cav}}} \right)^{1/2}, \quad (62)$$

where the dimensionless factors  $R_{\text{cav}}$  and  $L_{\text{cav}}$  are

$$R_{\text{cav}} = \frac{1}{M_e \omega_e^2} \left( \frac{\prod_{n=0}^{\infty} \lambda_n^o}{\prod_{n=2}^{\infty} \lambda_n} \right)^{1/2} \quad (63)$$

and

$$L_{\text{cav}} = \frac{M_e}{2} \left[ \int d\tau \left( \frac{d\bar{q}}{d\tau} \right)^2 \right]^{1/2} \left[ \int d\tau' \left( \frac{d\bar{q}}{d\tau'} \right)^2 \right]^{1/2}, \quad (64)$$

respectively. The exponent  $S_{B,1}^{\text{cav}}$  is given by

$$S_{B,1}^{\text{cav}} = \int_{-\theta/2}^{\theta/2} d\tau \left[ \frac{M_e}{2} \left( \frac{dq(\tau)}{d\tau} \right)^2 + V_Q(q) \right]. \quad (65)$$

This exponent accounts for the contribution from the two transversal of the potential barrier. We note that the exponent  $S_{B,1}^{\text{cav}}$  of Eq. (65) does not contain the nonlocal contribution, as in Eq. (28), because this contribution is already included in the calculation of  $\mathcal{Z}_1$  [see Eq. (60)]. We now compute  $R_{\text{cav}}$ ,  $L_{\text{cav}}$ , and  $S_{B,1}^{\text{cav}}$ , separately, to determine the ground-state energy splitting  $\Delta_{\text{cav}}$ . To focus on the effects due to the junction-cavity

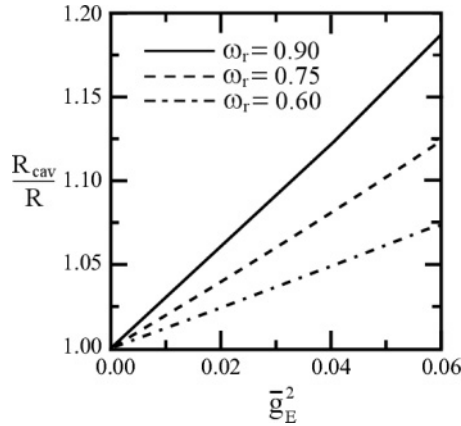


FIG. 11. The numerically computed ratio of the dimensionless factor  $R_{\text{cav}}/R$  is plotted as a function of the junction-cavity coupling strength  $\bar{g}_E^2$  for  $\omega_r = 0.60$  (dot-dashed line), 0.75 (dashed line), and 0.90 (solid line).

interaction, we present the details of the calculation for  $R_{\text{cav}}$  and  $L_{\text{cav}}$  in Appendixes A and B, respectively, and discuss the dependence of these factors on the junction-cavity coupling strength  $\bar{g}_E^2$ .

The dimensionless factor  $R_{\text{cav}}$  in the weak-coupling regime is given by

$$R_{\text{cav}} \cong 2 + \frac{\pi \bar{g}_E^2 \omega_r^2}{2M\omega_o^2} \frac{X_R}{(\omega_r + \omega_o)^3}, \quad (66)$$

where  $X_R = \omega_r^3 + 15\omega_r^2\omega_o + 12\omega_r\omega_o^2 - 2\omega_o^3$ . Equation (66) yields the value  $R_{\text{cav}} = 2$  in the absence of a resonant cavity (i.e.,  $\bar{g}_E^2 = 0$ ).<sup>38</sup> In Fig. 11, we plot the numerically computed ratio  $R_{\text{cav}}/R$  as a function of  $\bar{g}_E^2$  for  $\omega_r = 0.60$  (dot-dashed line), 0.75 (dashed line), and 0.90 (solid line) to illustrate enhancement of  $R$  due to the resonant cavity. The curves indicate that  $R_{\text{cav}}/R$  increases from 1 almost linearly with increasing  $\bar{g}_E^2$  and  $\omega_r$ .

For the dimensionless factor  $L_{\text{cav}}$ , we evaluate the integral of Eq. (64) by expanding the function  $Q(\tau)$ , which accounts for the nonlocal contribution to the bouncelike trajectory as a power series. (See Appendix B.) In the weak-coupling regime (i.e.,  $\bar{g}_E^2 \ll 1$ ), we obtain

$$L_{\text{cav}} \approx \mathcal{V}_M [A_o + \bar{g}_E^2 (B_o + B_2 q_o^2 + B_4 q_o^4)], \quad (67)$$

by retaining the leading-order contribution (in  $\bar{g}_E^2$ ). Here  $\mathcal{V}_M = q_o \sqrt{2M V_o}$ ,  $A_o = 1 - q_o^2(2\epsilon b_1/3V_o) - q_o^4(4\epsilon b_2/15V_o)$ ,  $B_o = -(\epsilon + 8b_3\omega_r^2)/8\epsilon$ ,  $B_2 = [b_1\epsilon + 2(6b_1b_3 - 1)\omega_r^2 + 2\pi d_1\omega_r^3]/6V_o$ , and  $B_4 = (b_2\epsilon + 20b_2b_3\omega_r^2 + 3\pi d_3\omega_r^3)/15V_o$ . The frequency-independent constants  $b_i$  are  $b_1 = (\cosh \ell - 2)\text{sech}^4(\ell/2)$ ,  $b_2 = (\cosh 2\ell - 26 \cosh \ell + 33)/(\cosh \ell + 1)^3$ , and  $b_3 = (\sinh \ell \tanh \ell)^2/(\cosh 2\ell - 7)$ . Equation (67) indicates that  $L_{\text{cav}}$  in the resonant cavity is larger than  $L = \mathcal{V}_M A_o$  in its absence. However, due to the functional form of  $L_{\text{cav}}$ , the enhancement of  $L_{\text{cav}}$  from  $L$  deviates from the linear dependence on  $\bar{g}_E^2$  at a smaller value than that for  $R_{\text{cav}}$ . To illustrate this deviation, we numerically compute  $L_{\text{cav}}$  and plot the ratio  $L_{\text{cav}}/L$  in Fig. 12 as a function of  $\bar{g}_E^2$  for  $\omega_r = 0.60$  (dot-dashed line), 0.75 (dashed line), and 0.90 (solid line). The curves show nonlinear enhancement of the dimensionless

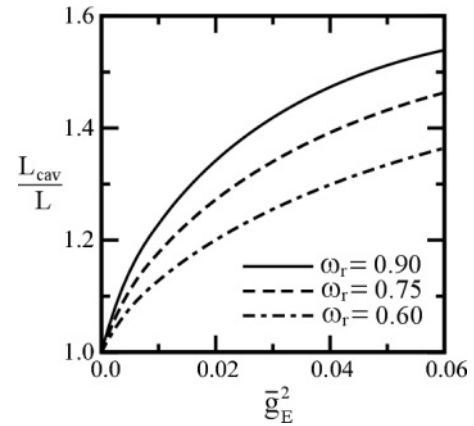


FIG. 12. The numerically computed ratio of  $L_{\text{cav}}/L$  is plotted as a function of the junction-cavity coupling strength  $\bar{g}_E^2$  for  $\omega_r = 0.60$  (dot-dashed line), 0.75 (dashed line), and 0.90 (solid line) to illustrate the enhancement.

factor  $L_{\text{cav}}$  for much smaller values of  $\bar{g}_E^2$  than that for  $R_{\text{cav}}$  shown in Fig. 11.

Finally, we estimate the effects of the junction-cavity interaction on  $S_{B,1}^{\text{cav}}$ . The action  $S_{B,1}^{\text{cav}}$  of Eq. (65) for the bouncelike trajectory is given by

$$S_{B,1}^{\text{cav}} = 2 \int_{(q_o/2)_-}^{(q_o/2)_+} dq \sqrt{2M_e V_Q(q)}. \quad (68)$$

The integral of Eq. (68) is evaluated in the same way as that for  $L_{\text{cav}}$  (see Appendix B). Again, we simplify the calculation by writing  $V_Q$  as a power series in  $q$  and then expand  $\sqrt{V_Q(q)}$  in powers of  $\bar{g}_E^2$  as

$$\sqrt{V_Q} \approx \frac{\mathcal{V}_M}{\sqrt{2M_e q_o}} \left\{ 1 - \frac{2\epsilon q^2}{V_o} \left( b_1 + \frac{4b_2}{3} q^2 + \dots \right) - \bar{g}_E^2 \left[ \frac{1}{8} + \frac{\omega_r^2 q_o^2}{2V_o} - \frac{\epsilon q^2}{2V_o} \left( \bar{b}_1 + \frac{2}{3} b_2 q^2 \right) \right] \right\}, \quad (69)$$

where  $\bar{b}_1 = b_1 + (\omega_r^2/\epsilon)$ . Using this series expansion for  $\sqrt{V_Q}$ , we evaluate Eq. (68) and obtain  $S_{B,1}^{\text{cav}}$  to the leading order in  $\bar{g}_E^2$  as

$$S_{B,1}^{\text{cav}} \approx 4\mathcal{V}_M [A_o + \bar{g}_E^2 (B_o + \bar{B}_2 q_o^2 + \bar{B}_4 q_o^4)], \quad (70)$$

where  $\bar{B}_2 = B_2 - (\pi d_1 \omega_r^3/3V_o)$  and  $\bar{B}_4 = B_4 - (3\pi d_3 \omega_r^3/15V_o)$ . The action  $S_{B,1}^{\text{cav}}$  in the presence of the cavity is reduced from that in its absence (i.e.,  $S_{B,1}^{\text{cav}} < S_{B,1}$ ). To illustrate this suppression of the ratio, we plot the numerically computed ratio  $S_{B,1}^{\text{cav}}/S_{B,1}$  as a function of  $\bar{g}_E^2$  for  $\omega_r = 0.60$  (dot-dashed line), 0.75 (dashed line), and 0.90 (solid line) in Fig. 13. The curves indicate that in the one-bounce contribution, the action decreases almost linearly with  $\bar{g}_E^2$  in the weak-coupling region as indicated by Eq. (70). This reduction reflects that the potential barrier height is reduced (see Fig. 9) and the potential minima become closer together (see Fig. 10) with increasing junction-cavity interaction strength.

We now combine the effects of the resonant cavity on  $R_{\text{cav}}$ ,  $L_{\text{cav}}$ , and  $S_{B,1}$  together and estimate the enhancement of the ground-state energy splitting  $\Delta_{\text{cav}}$  from  $\Delta$ . Here,  $\Delta$  denotes

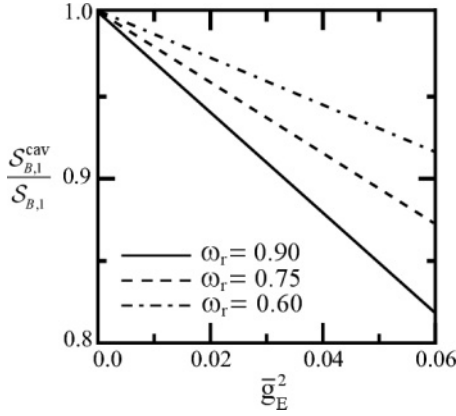


FIG. 13. The numerically computed ratio of the action  $S_{B,1}^{\text{cav}}/S_{B,1}$  is plotted as a function of  $\bar{g}_E^2$  for  $\omega_r = 0.60$  (dot-dashed line), 0.75 (dashed line), and 0.90 (solid line) to illustrate that the one-bounce-like action is reduced.

the energy splitting in the absence of a resonant cavity given by

$$\Delta = 2\mathcal{A} \left( \frac{S_o}{2\pi} \right)^{1/2} e^{-S_o}, \quad (71)$$

where  $\mathcal{A} = [\prod_{n=0}^{\infty} \lambda_n^o / \prod_{n=1}^{\infty} \lambda_n]^{1/2}$  and  $S_o$  denotes the action integral. In the weak-coupling regime, the ratio  $\Delta_{\text{cav}}/\Delta$  to the leading order in  $\bar{g}_E^2$  is given by

$$\begin{aligned} \frac{\Delta_{\text{cav}}}{\Delta} \approx & 1 + \frac{\bar{g}_E^2}{M} \left\{ 1 + \frac{\omega_r^2}{\omega_o^2} \left[ 1 - \Upsilon + \frac{\pi X_R}{8(\omega_r + \omega_o)^3} \right] \right. \\ & + \frac{M}{2A_o} (B_0 + B_2 q_o^2 + B_4 q_o^4) \\ & \left. - 2M\mathcal{V}_M (B_0 + \bar{B}_2 q_o^2 + \bar{B}_4 q_o^4) \right\}. \quad (72) \end{aligned}$$

The result indicates that  $\Delta_{\text{cav}}$  is enhanced with increasing  $\bar{g}_E^2$  and  $\omega_r$ . To illustrate this enhancement, we numerically compute and plot  $\Delta_{\text{cav}}/\Delta$  as a function of  $\bar{g}_E^2$  for  $\omega_r = 0.60$  (dot-dashed line), 0.75 (dashed line), and 0.90 (solid line) in Fig. 14. The curves show that  $\Delta_{\text{cav}}/\Delta$  increases roughly

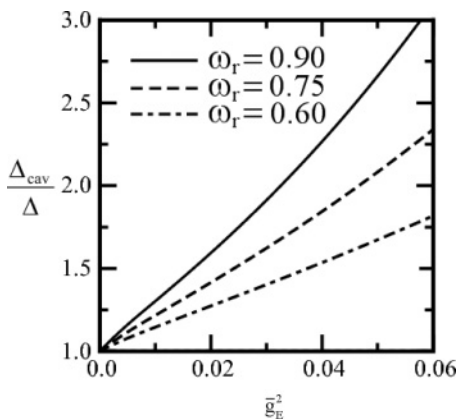


FIG. 14. The numerically computed ratio of  $\Delta_{\text{cav}}/\Delta$  is plotted as a function of the junction-cavity coupling strength  $\bar{g}_E^2$  for  $\omega_r = 0.60$  (dot-dashed line), 0.75 (dashed line), and 0.90 (solid line) to illustrate the enhancement in a resonant cavity.

linearly with  $\bar{g}_E^2$  from  $\bar{g}_E^2 = 0$  to 0.02. However, the deviation from this linear behavior becomes noticeable for  $\bar{g}_E^2 \geq 0.02$ . Also,  $\Delta_{\text{cav}}/\Delta$  increases significantly from 1 at  $\bar{g}_E^2 = 0$  in the weak-coupling regime. We note that the corresponding changes in the ratio  $R_{\text{cav}}/R$ ,  $L_{\text{cav}}/L$ , and  $S_{B,1}^{\text{cav}}/S_{B,1}$  over the same range of  $\bar{g}_E^2$  are less significant. For instance,  $\Delta_{\text{cav}}/\Delta$  for  $\omega_r = 0.90$  increases from 1.0 to 1.45 for the increase of  $\bar{g}_E^2$  from 0.0 to 0.015. Over the same range of  $\bar{g}_E^2$ ,  $R_{\text{cav}}/R$ ,  $L_{\text{cav}}/L$ , and  $S_{B,1}^{\text{cav}}/S_{B,1}$  change from 1.0 to 1.05, from 1.0 to 1.29, and from 1.0 to 0.96, respectively. The notable increase in  $\Delta_{\text{cav}}/\Delta$  compared to  $R_{\text{cav}}/R$ ,  $L_{\text{cav}}/L$ , and  $S_{B,1}^{\text{cav}}/S_{B,1}$  reflects that  $\Delta$  is small.<sup>3</sup> Hence,  $\Delta_{\text{cav}}$  depends sensitively on the variation of the exponent  $S_{B,1}^{\text{cav}}$ .

## VI. SUMMARY AND CONCLUSION

In summary, we investigated the effects of a high- $Q_c$  resonant cavity on MQT of fluxons from a metastable state in a single LJJ and in a stack of two coupled LJJ's. Also, we estimated the ground-state energy splitting for fluxons in a double-well potential. We find that both the tunneling rate and the ground-state energy splitting are increased in the resonant cavity. However, the amount of these increases is significantly different. For MQT of the fluxon, the tunneling rate increases due to the renormalization of fluxon mass, but is negligible in the weak-coupling regime. On the other hand, the increase in the ground-state energy splitting is due to potential renormalization, but this increase can become significant with increasing  $\bar{g}_E^2$ , as shown in Fig. 14. This energy splitting enhancement is consistent with the result of an increase in the energy separation due to the interaction between a two-level system and a quantized radiation field, described by the Jaynes-Cummings (JC) model.<sup>27</sup> Moreover, the consistency<sup>41</sup> between the result of the present work and that of the JC model indicates that the effective Hamiltonian for the JVQ-cavity system may be similar to the JC model.

The effects due to (i) interaction between the JVQ and a dissipative environment and (ii) the losses resulting from a low- $Q$  cavity are neglected in the present work. These dissipative effects are expected to be present in real systems and may be accounted for by using an effective spectral density that characterizes the form of dissipation.<sup>42</sup> Inclusion of both the dissipative environment and cavity losses may reduce the size of the increase in the ground-state energy splitting and may lead to a decrease in the energy splitting when the dissipative effects become strong, as indicated by an analysis of dissipative two-state systems.<sup>30</sup> However, these dissipation contributions do not reverse the effects due to the potential renormalization completely in weakly dissipative systems.

Enhancement of the ground-state energy splitting due to the junction-cavity interaction may have an important consequence for the decoherence time of JVQ in the resonant cavity. Earlier study<sup>3</sup> of the JVQ decoherence time by Kim, Dhungana, and Park indicates that the increase in the decoherence time in a noisy environment (i.e.,  $T_\phi^{\text{noise}}$ ) is correlated with the increasing ground-state energy splitting  $\Delta$ . This suggests that, as  $\Delta$  may be tuned by adjusting the strength of the junction-cavity interaction, the resonant cavity may be used to control the property of the JVQ. For instance,

the decoherence time  $T_\phi^{\text{noise}}$  may be increased by increasing the strength of the interaction between the fluxon and the cavity EM mode. Also, due to the similarities between a cavity EM mode and an optical phonon mode, the interaction between fluxons and optical phonons in the LJJ may affect the decoherence time.

Another important property of JVQ's is entanglement between the qubits. As our result suggests that the decoherence time for the JVQ can be increased by increasing the strength of the junction-cavity interaction, the resonant cavity may also be useful for tuning the level of entanglement between the JVQ's. Our study suggests that the present approach for JVQ's is similar to the microwave cavity approach used for the other superconductor qubits.<sup>43</sup> The effective Hamiltonian for the multiple JVQ's in a resonant cavity may resemble the Tavis-Cummings model,<sup>44</sup> which is the extension of the JC model to the case of multiple qubits. This similarity may be exploited by using the resonant cavity to control the level of concurrence<sup>45</sup> for JVQ's since the junction-cavity interaction may also promote entanglement. Hence, the effects of a resonant cavity on entanglement between the interacting JVQ's would be an interesting area for further study.

#### ACKNOWLEDGMENTS

The authors would like to thank W. Schwalm and K.-S. Park for helpful discussions and I. D. O'Bryant for assisting with part of the numerical calculation.

#### APPENDIX A: CALCULATION OF $R_{\text{cav}}$

For convenience, the dimensionless factor  $R_{\text{cav}}$  of Eq. (63) is estimated in the continuum limit. In this limit, we may write  $R_{\text{cav}}$  as

$$R_{\text{cav}} = \exp \left\{ \frac{1}{\pi} \int_{M_e \omega_e^2}^{\infty} \frac{d\lambda}{\lambda} [\delta_+(\lambda) + \delta_-(\lambda)] \right\}, \quad (\text{A1})$$

where  $\delta_\pm(\lambda)$  denotes the phase shift due to the scattering potential  $U$ . This phase shift may be expressed as

$$\delta_\pm(\lambda) = \cot^{-1} \left[ \frac{U^{-1} - g'_\lambda(0) \mp g'_\lambda(\tau_s)}{g''_\lambda(0) \pm g''_\lambda(\tau_s)} \right], \quad (\text{A2})$$

where  $\tau_s = -\theta/2$ , and  $g'_\lambda(\tau)$  and  $g''_\lambda(\tau)$  denote the real and imaginary part of the Green's function [i.e.,  $g_\lambda(\tau) = g'_\lambda(\tau) + i g''_\lambda(\tau)$ ]. The phase shift  $\delta_\pm(\lambda)$  due to the scattering from the net potential difference of

$$V_Q''(\bar{q}) - V_Q''[(q_o/2)_-] = -U \left[ \delta \left( \tau + \frac{\tau_s}{2} \right) + \delta \left( \tau - \frac{\tau_s}{2} \right) \right] \quad (\text{A3})$$

consists of two Dirac  $\delta$  functions at  $\tau = \pm \tau_s/2$ . The strength of the scattering potential  $U$  is given by

$$U^{-1} = g_0(0) - g_0(\tau_s), \quad (\text{A4})$$

where  $g_0(\tau)$  is the Green's function for the eigenvalue  $\lambda = 0$ . The Green's function  $g_\lambda(\tau)$  is written as

$$g_\lambda(\tau) = \int_{-\infty}^{\infty} \frac{d\omega}{2\pi} \frac{e^{i\omega\tau}}{M_e[\omega^2 + \zeta(\omega) + \omega_e^2] - \lambda - i\delta}. \quad (\text{A5})$$

Here the effects of the resonant cavity are accounted for via  $M_e$ ,  $\omega_e$ , and  $\zeta(\omega)$ . The function  $\zeta(\omega)$ , obtained from the cavity kernel  $K(\tau)$  of Eq. (26),

$$\zeta(\omega) = \frac{4\pi \bar{g}_E^2 \omega_r^4}{M_e \omega^2 + \omega_r^2}, \quad (\text{A6})$$

reflects that the resonant cavity supports a single mode with frequency  $\omega_r$ . Using the function  $\zeta(\omega)$ , we write the real part of the Green's function as  $g'_\lambda(\tau) = g'_{\lambda,+}(\tau) + g'_{\lambda,-}(\tau)$ , where

$$g'_{\lambda,\pm}(\tau) = \frac{-1}{4M_e \omega_{\lambda,\pm}} \left( 1 \pm \frac{\omega_r^2 + \omega_{1,\lambda}^2}{2\omega_{2,\lambda}^2} \right) \sin \omega_{\lambda,\pm} \tau, \quad (\text{A7})$$

$\omega_{\lambda,\pm} = (\omega_{1,\lambda}^2 \pm \omega_{2,\lambda}^2)^{1/2}$ ,  $\omega_{1,\lambda}^2 = [(\lambda/M_e) - \omega_e^2 - \omega_r^2]/2$ , and  $\omega_{2,\lambda}^2 = \{[(\lambda/M_e) - \omega_e^2 + \omega_r^2]^2 - (16\pi \bar{g}_E^2/M_e) \omega_r^4\}^{1/2}$ . On the other hand, we write the imaginary part of the Green's function as  $g''_\lambda(\tau) = g''_{\lambda,+}(\tau) + g''_{\lambda,-}(\tau)$ , where

$$g''_{\lambda,\pm}(\tau) = \frac{1}{4M_e \omega_{\lambda,\pm}} \left( 1 \pm \frac{\Omega^2 + \omega_{1,\lambda}^2}{2\omega_{2,\lambda}^2} \right) \cos \omega_{\lambda,\pm} \tau. \quad (\text{A8})$$

We note that the phase shift  $\delta_\pm(\lambda)$  has both slowly varying and rapidly oscillating contributions. For an extended bounce (i.e.,  $\omega_e \tau_s \gg 1$ ), the rapidly oscillating terms become negligible compared to the nonoscillating terms.

The factor  $R_{\text{cav}}$  of Eq. (A1) may be simplified by using the substitution  $\lambda = M_e \omega_e^2 (1 + p^2)$ , where  $p$  is a dimensionless momentum variable. With this change of variable, we write  $R_{\text{cav}}$  as

$$R_{\text{cav}} = \exp \left\{ \frac{1}{\pi} \int_0^\infty \frac{p dp}{1 + p^2} [\delta_+(p) + \delta_-(p)] \right\}. \quad (\text{A9})$$

The factor  $R_{\text{cav}}$  of Eq. (A9) may be further simplified by neglecting the rapidly oscillating contributions in the phase shift  $\delta_\pm(\lambda)$  of Eq. (A2). Neglecting these oscillatory contributions, we approximate  $\delta_\pm(p)$  to a simpler form  $\delta(p)$  and write the factor  $R_{\text{cav}}$  as

$$R_{\text{cav}} = \exp \left\{ \frac{2}{\pi} \int_0^\infty \frac{p dp}{1 + p^2} \delta(p) \right\}. \quad (\text{A10})$$

The simplified phase shift  $\delta(p)$  is given by

$$\delta(p) = \cot^{-1} \left[ \frac{U^{-1} - g'_p(0)}{g''_p(0)} \right], \quad (\text{A11})$$

where the scattering potential strength  $U$  is given by

$$U^{-1} = \frac{1}{4M_e} \left( \frac{1 - W_0}{\sqrt{\omega_{2,0}^2 - \omega_{1,0}^2}} + \frac{1 + W_0}{\sqrt{\omega_{2,0}^2 + \omega_{1,0}^2}} \right), \quad (\text{A12})$$

and  $W_0 = (\omega_r^2 + \omega_{1,0}^2)/\omega_{2,0}^2$ . We note that  $\omega_{1,0}$  and  $\omega_{2,0}$  are obtained from  $\omega_{1,\lambda}$  and  $\omega_{2,\lambda}$  of Eq. (A7) for the eigenvalue  $\lambda = 0$ , respectively. The real and imaginary part of the Green's function are given, respectively, by

$$g'_p(0) = \frac{1}{4M_e} \frac{1 - W_p}{\sqrt{\omega_{2,p}^2 - \omega_{1,p}^2}} \quad (\text{A13})$$



and

$$g_p''(0) = \frac{1}{4M_e} \frac{1 + W_p}{\sqrt{\omega_{2,p}^2 + \omega_{1,p}^2}}, \quad (\text{A14})$$

where  $W_p = (\omega_r^2 + \omega_{1,p}^2)/\omega_{2,p}^2$ . We note that  $\omega_{1,p}$  and  $\omega_{2,p}$  are obtained from  $\omega_{1,\lambda}$  and  $\omega_{2,\lambda}$  of Eq. (A7), respectively, by setting  $\lambda = M_e \omega_e^2 (1 + p^2)$ .

We now compute  $R_{\text{cav}}$  to the leading order in  $\bar{g}_E^2$  to account for the effects of a resonant cavity in the weak-coupling regime (i.e.,  $\bar{g}_E^2 \ll 1$ ). For this calculation, we write the renormalized mass of the fluxon as  $M_e = M - 2\bar{g}_E^2$  and express the oscillation frequency  $\omega_e$  as

$$\omega_e^2 \cong \omega_o^2 \left\{ 1 + \frac{2\bar{g}_E^2}{M} \left[ 1 + \frac{\omega_r^2}{\omega_o^2} (1 - \Upsilon) \right] \right\}. \quad (\text{A15})$$

Also we rewrite the strength of the potential  $U$  as

$$U^{-1} \cong \frac{1}{2M\omega_o} - \frac{2\pi\bar{g}_E^2\omega_r^3}{M^2(\omega_r^2 - \omega_o^2)^2} \left( 1 - \frac{X_u}{32\pi\omega_r^3\omega_o^3} \right), \quad (\text{A16})$$

where  $X_u = M\omega_o^2(\omega_o^2 - \omega_r^2)^2 - 8[\omega_r^2\Upsilon(\omega_o^2 - \omega_r^2)^2 + 2\pi\omega_r^4(\omega_r^2 - 3\omega_o^2)]$ . By combining these expressions, we rewrite the real and imaginary part of the Green's function of Eqs. (A13) and (A14), respectively, as

$$g_p'(0) \cong -\frac{\bar{g}_E^2\pi\omega_r^3}{2M^2(p^2\omega_o^2 + \omega_r^2)^2} \quad (\text{A17})$$

and

$$g_p''(0) = \frac{1}{2Mp\omega_o} \left[ 1 + \frac{\bar{g}_E^2 X_g}{8Mp^2\omega_o^2(p^2\omega_o^2 + \omega_r^2)^2} \right], \quad (\text{A18})$$

where  $X_g = 4\omega_r^2[\pi\omega_o^2(3p^2\omega_o^2 + \omega_r^2) - 2\Upsilon p^2(p^2\omega_o^2 + \omega_r^2)^2] + Mp^2\omega_o^2(p^2\omega_o^2 + \omega_r^2)^2$ . Now, we use Eqs. (A16)–(A18) and rewrite the simplified phase shift  $\delta(p)$  of Eq. (A11) as

$$\delta(p) \cong \cot^{-1} p - \frac{\bar{g}_E^2\pi\omega_r^3 X_p}{2Mp(1 + p^2)X_\omega}, \quad (\text{A19})$$

where  $X_p = -(\omega_o^2\omega_r^3 + 2\omega_o\omega_r^4 + \omega_r^5) + p^2(2\omega_o^5 + \omega_r^4\omega_r - 4\omega_o^3\omega_r^2 - 3\omega_o^2\omega_r^3 - 8\omega_o\omega_r^4 - 4\omega_r^5) - p^4(16\omega_o^3\omega_r^2 + 8\omega_o^2\omega_r^3) - p^6(8\omega_o^5 + 4\omega_o^4\omega_r)$  and  $X_\omega = \omega_o^2(\omega_o + \omega_r)^2(p^2\omega_o^2 + \omega_r^2)^2$ . Finally, we substitute  $\delta(p)$  of Eq. (A19) into  $R_{\text{cav}}$  of Eq. (A10) and evaluate the integral to obtain

$$R_{\text{cav}} \cong 2 + \frac{\pi\bar{g}_E^2\omega_r^2}{2M\omega_o^2} \frac{X_R}{(\omega_r + \omega_o)^3}, \quad (\text{A20})$$

where  $X_R = 5\omega_r^3 + 15\omega_r^2\omega_o + 12\omega_r\omega_o^2 - 2\omega_o^3$ . Equation (A20) yields  $R_{\text{cav}} = 2$  in the absence of the resonant cavity (i.e.,  $\bar{g}_E^2 = 0$ ) as expected.<sup>38</sup>

#### APPENDIX B: CALCULATION OF $L_{\text{cav}}$

The factor  $L_{\text{cav}}$  of Eq. (64) may be estimated by determining the bouncelike trajectories  $q(\tau)$ . The trajectories obey the

equation of motion given by

$$-M_e \frac{d^2 q(\tau)}{d\tau^2} + \frac{dV_Q(q)}{dq} + 4\pi\bar{g}_E^2 \int_{-\infty}^{\infty} d\tau' K(\tau - \tau') q(\tau) = 0. \quad (\text{B1})$$

We rewrite the equation of motion in a convenient form by integrating Eq. (B1) by parts and obtain

$$-\frac{M_e}{2} \left( \frac{dq}{d\tau} \right)^2 + V_Q(q) + 4\pi\bar{g}_E^2 \int_{-\infty}^{\infty} d\tau' K(\tau - \tau') q(\tau) q(\tau') = 0. \quad (\text{B2})$$

Using this result, we write the factor  $L_{\text{cav}}$  as

$$L_{\text{cav}} \approx \frac{M_e}{2} \int d\tau \left( \frac{dq}{d\tau} \right)^2 = \int_{(q_o/2)_-}^{(q_o/2)_+} dq \sqrt{V_Q(q) + 2\pi\bar{g}_E^2\omega_r^2 Q(\tau)}, \quad (\text{B3})$$

where  $q = q(\tau)$  and

$$Q(\tau) = \int_{-\infty}^{\infty} d\tau' e^{-\omega_r|\tau - \tau'|} q(\tau'). \quad (\text{B4})$$

Here, the nonlocal contribution due to the resonant cavity is accounted for by  $Q(\tau)$ . As discussed in Appendix C, the function  $Q(\tau)$  is similar to  $q(\tau)$ . By exploiting this similarity, we expand  $Q(\tau)$  in a power series as

$$Q(\tau) = \sum_{n=0}^{\infty} d_{2n+1} q^{2n+1}(\tau), \quad (\text{B5})$$

where  $d_{2n+1}$  is the expansion coefficients (see Appendix C). The power-series expansion for  $Q(\tau)$  allows us to evaluate the factor  $L_{\text{cav}}$  straightforwardly. By using this power-series expansion, we evaluate the integral of Eq. (B3) in the weak-coupling regime (i.e.,  $\bar{g}_E^2 \ll 1$ ) and obtain the factor  $L_{\text{cav}}$  to the leading order in  $\bar{g}_E^2$  as

$$L_{\text{cav}} \approx \mathcal{V}_M [A_o + \bar{g}_E^2 (B_o + B_2 q_o^2 + B_4 q_o^4)], \quad (\text{B6})$$

where  $\mathcal{V}_M = q_o \sqrt{2M V_o}$ ,  $A_o = 1 - q_o^2(2\epsilon b_1/3V_o) - q_o^4(4\epsilon b_2/15V_o)$ ,  $B_o = -(\epsilon + 8b_3\omega_r^2)/8\epsilon$ ,  $B_2 = [b_1\epsilon + 2(6b_1b_3 - 1)\omega_r^2 + 2\pi d_1\omega_r^3]/6V_o$ , and  $B_4 = (b_2\epsilon + 20b_2b_3\omega_r^2 + 3\pi d_3\omega_r^3)/15V_o$ . The frequency-independent constants  $b_i$  are given by  $b_1 = (\cosh \ell - 2)\text{sech}^4(\ell/2)$ ,  $b_2 = (\cosh 2\ell - 26 \cosh \ell + 33)/(\cosh \ell + 1)^3$ , and  $b_3 = (\sinh \ell \tanh \ell)^2/(\cosh 2\ell - 7)$ .

#### APPENDIX C: POWER-SERIES EXPANSION OF $Q(\tau)$

The numerically computed function  $Q(\tau)$  of Eq. (B4) indicates that  $Q(\tau)$  is similar to the functional form of the bouncelike trajectory  $q(\tau)$ . This similarity suggests that  $Q(\tau)$  is a scaled function of  $q(\tau)$  as shown schematically in Fig. 15. In this case, we may express the function  $Q(\tau)$  as a power series in  $q(\tau)$  as

$$Q(\tau) = \sum_{n=0}^{\infty} d_{2n+1} q^{2n+1}(\tau), \quad (\text{C1})$$

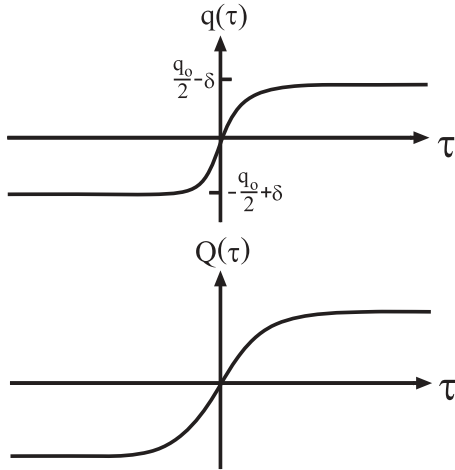


FIG. 15. The similarity between the function  $Q(\tau)$  of Eq. (B4) and the instanton solution  $q(\tau)$  representing the trajectory of the fluxon from one potential minimum to the other via tunneling is illustrated schematically.

where  $d_{2n+1}$  denotes the coefficient for this power-series expansion. We compute the coefficients  $d_{2n+1}$  by starting with a series expansion of  $q(\tau)$  in  $\tau$  as

$$q(\tau) = \sum_{n=0}^{\infty} a_{2n+1} \tau^{2n+1}, \quad (\text{C2})$$

noting that the instanton solution  $q(\tau)$  is an odd function of  $\tau$ . Here, the coefficient  $d_{2n+1}$  is obtained by following the five steps as discussed later in this appendix. First, we write the bouncelike trajectory  $q$  in the absence of a resonant cavity. This trajectory  $q$  may be expressed as

$$q = -b_1 \tau + b_2 \tanh^{-1}(b_3 \tanh q), \quad (\text{C3})$$

where the constants  $b_1 = 2\sqrt{\epsilon/M} \coth \ell$ ,  $b_2 = (\cosh 2q_o + \cosh \ell) / \sinh 2q_o$ , and  $b_3 = \coth q_o$  depend on the parameters  $\ell$  and  $\epsilon$ . Second, we expand the right-hand side of Eq. (C3) as a power series in  $q$  as

$$q = -b_1 \tau + b_2 b_3 q \left( 1 - \frac{1 - b_3^2}{3} q^2 + \frac{2 - 5b_3^2 + 3b_3^4}{15} q^4 + \dots \right). \quad (\text{C4})$$

Here, we find the coefficients  $a_{2n+1}$  by substituting the series expansion for  $q(\tau)$  of Eq. (C2) into Eq. (C4). The first three coefficients are given by

$$\begin{aligned} a_1 &= \frac{b_1}{b_2 b_3 - 1}, \\ a_3 &= \frac{b_1^3 b_2 b_3 (1 - b_3^2)}{3(b_2 b_3 - 1)^4}, \\ a_5 &= \frac{b_1^5 b_2 b_3 (1 - b_3^2) [b_2 b_3 (3 - 2b_3^2) + (2 - 3b_3^2)]}{15(b_2 b_3 - 1)^7}. \end{aligned}$$

Third, we use Eqs. (26) and (C2) to evaluate  $Q(\tau)$  of Eq. (B4) explicitly as

$$Q(\tau) = \sum_{n=0}^{\infty} a_{2n+1} \int_0^{\infty} d\tau' e^{-\omega_r |\tau - \tau'|} \tau'^{2n+1}. \quad (\text{C5})$$

Fourth, we evaluate the integrals of Eq. (C5) and write  $Q(\tau)$  in a power series in  $\tau$  as

$$\begin{aligned} Q(\tau) \approx \frac{2}{\omega_r} \left[ \tau \left( a_1 + \frac{6a_3}{\omega_r^2} + \frac{120a_5}{\omega_r^4} \right) \right. \\ \left. + \tau^3 \left( a_3 + \frac{20a_5}{\omega_r^2} \right) + \tau^5 a_5 + \dots \right]. \quad (\text{C6}) \end{aligned}$$

Finally, we use the power-series expansion for  $q(\tau)$  of Eq. (C2) and rewrite  $Q(\tau)$  of Eq. (C1) as

$$\begin{aligned} Q(\tau) = \tau(d_1 a_1) + \tau^3(d_1 a_3 + d_3 a_3^3) \\ + \tau^5(d_1 a_5 + 3d_3 a_1^2 a_3 + d_5 a_1^5) + \dots \quad (\text{C7}) \end{aligned}$$

This series expansion allows us to obtain the expansion coefficients  $d_{2n+1}$  by comparing the power series  $Q(\tau)$  of Eqs. (C6) and (C7). The first three expansion coefficients,  $d_{2n+1}$ , are the following:

$$\begin{aligned} d_1 &= \frac{2}{\omega_r} \left( 1 + \frac{6}{\omega_r^2} \frac{a_3}{a_1} + \dots \right), \\ d_3 &= \frac{4}{\omega_r^3} \left[ \left( \frac{10a_5}{a_1^3} - \frac{3a_3^2}{a_1^4} \right) + \frac{60}{\omega_r^4} \left( \frac{7a_7}{a_1^3} - \frac{a_3 a_5}{a_1^4} \right) + \dots \right], \\ d_5 &= \frac{12}{\omega_r^3} \left[ \left( \frac{7a_7}{a_1^5} - \frac{11a_3 a_5}{a_1^6} + \frac{3a_3^3}{a_1^7} \right) + \dots \right]. \end{aligned}$$

In Sec. V, we use these expansion coefficients to estimate the dimensionless factor  $L_{\text{cav}}$  and the one-bounce contribution to the action (i.e.,  $S_{B,1}^{\text{cav}}$ ).

\*Present address: Department of Physics, University of Colorado, Denver, P.O. Box 173364, Denver, CO 80217.

<sup>1</sup>A. Wallraff, J. Lisenfeld, A. Lukashenko, A. Kemp, M. Fistul, Y. Koval, and A. V. Ustinov, *Nature (London)* **425**, 155 (2003).

<sup>2</sup>J. Clarke, *Nature (London)* **425**, 113 (2003); A. Kemp, A. Wallraff, and A. V. Ustinov, *Phys. Status Solidi B* **233**, 472 (2002).

<sup>3</sup>J. H. Kim, R. P. Dhungana, and K.-S. Park, *Phys. Rev. B* **73**, 214506 (2006).

<sup>4</sup>P. D. Shaju and V. C. Kuriakos, *Physica C* **424**, 125 (2005); G. Carapella, F. Russo, R. Latempa, and G. Costabile, *Phys. Rev. B* **70**, 092502 (2004); V. M. Kaurov and A. B. Kuklov, *Phys. Rev. A* **71**, 011601(R) (2005).

<sup>5</sup>Y. Nakamura, Y. A. Pashkin, and J. S. Tsai, *Nature (London)* **398**, 786 (1999); Y. A. Pashkin, T. Yamamoto, O. Astafiev, Y. Nakamura, D. V. Averin, and J. S. Tsai, *ibid.* **421**, 823 (2003).

<sup>6</sup>J. M. Martinis, S. Nam, J. Aumentado, and C. Urbina, *Phys. Rev. Lett.* **89**, 117901 (2002); Y. Yu, S. Han, X. Chu, S.-I. Chu, and Z. Wang, *Science* **296**, 889 (2002).

<sup>7</sup>J. R. Friedman, V. Pael, W. Chen, S. K. Tolpygo, and J. E. Lukens, *Nature (London)* **406**, 43 (2000); C. H. van der Wal, A. C. J. T. Haar, F. K. Wilhelm, R. N. Schouten, C. J. P. M. Harmans, T. P. Orlando, S. Lloyd, and J. E. Mooji, *Science* **290**, 773 (2000); I. Chiorescu, Y. Nakamura, C. J. P. M. Harmans, and J. E. Mooji, *ibid.* **299**, 1896 (2003).

- <sup>8</sup>A. N. Price, A. Kemp, D. R. Gulevich, F. V. Kusmartsev, and A. V. Ustinov, *Phys. Rev. B* **81**, 014506 (2010).
- <sup>9</sup>See, for example, G. P. Bermana, A. R. Bishop, A. A. Chumaka, C. D. Kiniond, and V. I. Tsifrinoviche, e-print [arXiv:0912.3791](https://arxiv.org/abs/0912.3791); F. W. Strauch, S. K. Dutta, H. Paik, T. A. Palomaki, K. Mitra, B. K. Cooper, R. M. Lewis, J. R. Anderson, A. J. Dragt, C. J. Lobb, and F. C. Wellstood, *IEEE Trans. Appl. Supercond.* **17**, 105 (2007); J. Majer, J. M. Chow, J. M. Gambetta, J. Koch, B. R. Johnson, J. A. Schreier, L. Frunzio, D. I. Schuster, A. A. Houck, A. Wallraff, A. Blais, M. H. Devoret, S. Girvin, and R. J. Schoelkopf, *Nature (London)* **449**, 443 (2007).
- <sup>10</sup>G. Yi-Bo and L. Chong, *Commun. Theor. Phys.* **43**, 213 (2005); S.-L. Zhu, Z. D. Wang, and K. Yang, *Phys. Rev. A* **68**, 034303 (2003); Y. X. Lui, L. F. Wei, and F. Nori, *ibid.* **72**, 033818 (2005).
- <sup>11</sup>E. Almaas and D. Stroud, *Phys. Rev. B* **65**, 134502 (2002).
- <sup>12</sup>I. Tornes and D. Stroud, *Phys. Rev. B* **71**, 144503 (2005).
- <sup>13</sup>Ch. Helm, Ch. Preis, Ch. Walter, and J. Keller, *Phys. Rev. B* **62**, 6002 (2000); Ch. Helm, Ch. Preis, F. Forsthofer, J. Keller, K. Schlenga, R. Kleiner, and P. Müller, *Phys. Rev. Lett.* **79**, 737 (1997).
- <sup>14</sup>S. Sakai, A. V. Ustinov, H. Kohlstedt, A. Petraglia, and N. F. Pedersen, *Phys. Rev. B* **50**, 12905 (1994).
- <sup>15</sup>J. H. Kim and J. Pokharel, *Physica C* **348**, 425 (2003).
- <sup>16</sup>R. Kleiner, P. Müller, H. Kohlstedt, N. F. Pedersen, and S. Sakai, *Phys. Rev. B* **50**, 3942 (1994).
- <sup>17</sup>A. Davidson and N. F. Pedersen, *Appl. Phys. Lett.* **60**, 2017 (1992).
- <sup>18</sup>A. Irie and G. Oya, *Physica C* **293**, 249 (1997).
- <sup>19</sup>S. Madsen and N. Grønbech-Jensen, *Phys. Rev. B* **71**, 132506 (2005); N. Grønbech-Jensen, N. F. Pedersen, A. Davidson, and R. D. Parmentier, *ibid.* **42**, 6035 (1990).
- <sup>20</sup>S. Madsen, G. Filatrella, and N. F. Pedersen, *Eur. Phys. J. B* **40**, 209 (2004).
- <sup>21</sup>A. O. Sboychakov, S. Savel'ev, and F. Nori, *Phys. Rev. B* **78**, 134518 (2008).
- <sup>22</sup>S. Madsen, N. F. Pedersen, and P. L. Christiansen, *Physica C* **468**, 649 (2008).
- <sup>23</sup>T. Kato and M. Imada, *J. Phys. Soc. Jpn.* **65**, 2963 (1996); H. Simanjuntak and L. Gunther, *Phys. Rev. B* **42**, 930 (1990).
- <sup>24</sup>A. Shnirman, E. Ben-Jacob, and B. A. Malomed, *Phys. Rev. B* **56**, 14677 (1997).
- <sup>25</sup>J. H. Kim and K. Moon, *Phys. Rev. B* **71**, 104524 (2005).
- <sup>26</sup>E. G. Maksimov, P. I. Arseyev, and N. S. Maslova, *Solid State Commun.* **111**, 391 (1999).
- <sup>27</sup>E. T. Jaynes and F. W. Cummings, *Proc. IEEE* **51**, 89 (1963).
- <sup>28</sup>D. W. McLaughlin and A. C. Scott, *Phys. Rev. A* **18**, 1652 (1978).
- <sup>29</sup>A. O. Caldeira and A. J. Leggett, *Ann. Phys. (NY)* **149**, 374 (1983); *Phys. Rev. Lett.* **46**, 211 (1981).
- <sup>30</sup>See, for example, A. J. Leggett, S. Chakravarty, A. Dorsey, M. A. P. Fisher, A. Garg, and W. Zwerger, *Rev. Mod. Phys.* **59**, 1 (1987).
- <sup>31</sup>J.-L. Gervais, A. Jevicki, and B. Sakita, *Phys. Rev. D* **12**, 1038 (1975).
- <sup>32</sup>C. Gorria, P. L. Christiansen, Yu. B. Gaididei, V. Muto, N. F. Pedersen, and M. P. Soerensen, *Phys. Rev. B* **68**, 035415 (2003); P. Wofo, *Phys. Lett. A* **302**, 137 (2002).
- <sup>33</sup>J. P. Sethna, *Phys. Rev. B* **24**, 698 (1981).
- <sup>34</sup>J. S. Langer, *Ann. Phys. (NY)* **41**, 108 (1967); C. G. Callan Jr. and S. Coleman, *Phys. Rev. D* **16**, 1762 (1977).
- <sup>35</sup>J. H. Kim, I. D. O'Bryant, and R. P. Dhungana (unpublished).
- <sup>36</sup>T. Banks, C. M. Bender, and T. T. Wu, *Phys. Rev. D* **8**, 3346 (1973).
- <sup>37</sup>H. Grabert, U. Weiss, and P. Hanggi, *Phys. Rev. Lett.* **52**, 2193 (1984).
- <sup>38</sup>A. Garg, *Am. J. Phys.* **68**, 430 (2000).
- <sup>39</sup>S. Coleman, *Aspects of Symmetry* (Cambridge University Press, Cambridge, 1985), p. 265.
- <sup>40</sup>U. Weiss, H. Grabert, P. Hanggi, and P. Riseborough, *Phys. Rev. B* **35**, 9535 (1987).
- <sup>41</sup>P. L. Knight and P. W. Milonni, *Phys. Rep.* **66**, 21 (1980); see also, for example, C. C. Gerry and P. L. Knight, *Introductory Quantum Optics* (Cambridge University Press, Cambridge, 2005).
- <sup>42</sup>A. Garg, J. Onuchic, and V. Ambegaokar, *J. Chem. Phys.* **83**, 4491 (1987); M. Murao and F. Shibata, *J. Phys. Soc. Jpn.* **64**, 2394 (1995).
- <sup>43</sup>J. Major, J. M. Chow, J. M. Gambetta, J. Koch, B. R. Johnson, J. A. Schreier, L. Frunzio, D. I. Schuster, A. A. Houck, A. Wallraff, A. Blais, M. H. Devoret, S. M. Girvin, and R. J. Schoelkopf, *Nature (London)* **449**, 443 (2007); M. Sillanpää, J. Park, and R. Simmonds, *ibid.* **449**, 438 (2007); J. M. Fink, R. Bianchetti, M. Baur, M. Göppl, L. Steffen, S. Filipp, P. J. Leek, A. Blais, and A. Wallraff, *Phys. Rev. Lett.* **103**, 083601 (2009).
- <sup>44</sup>M. Tavis and F. W. Cummings, *Phys. Rev.* **170**, 379 (1968).
- <sup>45</sup>S. Hill and W. K. Wootters, *Phys. Rev. Lett.* **78**, 5022 (1997).